**Article:**

Webb, AAG, Guo, H, Clift, PD et al. (7 more authors) (2017) The Himalaya in 3D: Slab dynamics controlled mountain building and monsoon intensification. Lithosphere, 9 (4). pp. 637-651. ISSN 1941-8264

https://doi.org/10.1130/L636.1

# The Himalaya in 3D: slab dynamics controlled mountain building and monsoon intensification

**A. Alexander G. Webb[1], Hongcheng Guo[2], Peter D. Clift[2], Laurent Husson[3], Thomas Müller[4], Diego Costantino[4], An Yin[5], Zhiqin Xu[6,7,8], Hui Cao[6], and Qin Wang[7]**

[1]Department of Earth Sciences and Laboratory for Space Research, University of Hong Kong, Hong Kong, China.

[2]Department of Geology and Geophysics, Louisiana State University, Baton Rouge LA 70803, USA.

[3]ISTerre, CNRS UMR 5275, Univ. Grenoble Alpes, F-38041 Grenoble, France.

[4]School of Earth and Environment, University of Leeds, Leeds LS2 9JT, UK.

[5]Department of Earth, Planetary, and Space Sciences and the Institute of Planets and Exoplanets, University of California, Los Angeles CA 90095, USA.

[6]Key Laboratory of Continental Tectonics and Dynamics, Institute of Geology, Chinese Academy of Geological Sciences, Beijing 100037, China.

[7]State Key Laboratory for Mineral Deposits Research, Department of Earth Sciences, Nanjing University, Nanjing 210046, China.

[8]School of Earth Sciences and Resources, China University of Geosciences (Beijing), Beijing 100083, China.

**Submitted To:** Lithosphere

**Original Submission Date:** 12 December 2016

**Re-submitted**: 7 March 2017

## ABSTRACT

Tectonic models for the Oligocene-Miocene development of the Himalayan Mountains are largely focused on crustal-scale processes, and developed along orogen-perpendicular cross sections. Such models assume uniformity along the length of the Himalaya, but significant along-strike tectonic variations occur, highlighting a need for three dimensional evolutionary models of Himalayan orogenesis. Here we show a strong temporal correlation of southward motion of the Indian slab relative to the over-riding Himalayan orogen, lateral migration of slab detachment, and subsequent dynamic rebound with major changes in Himalayan metamorphism, deformation, and exhumation. Slab detachment was also coeval with South Asian monsoon intensification, which leads us to hypothesize their genetic link. We further propose that anchoring of the Indian continental subducted lithosphere from 30 to 25 million years ago steepened the dip of the Himalayan sole thrust, resulting in crustal shortening deep within the Himalayan orogenic wedge. During the subsequent -'13 million years, slab detachment propagated inward from both Himalayan syntaxes. Resultant dynamic rebound terminated deep crustal shortening and caused a rapid rise of the mountain range. The increased orography intensified the South Asian monsoon. Decreased compressive forces in response to slab detachment may explain an observed -'25% decrease in the India-Eurasia convergence rate. The asymmetric curvature of the arc – broadly open, but tighter to the east – suggests faster slab detachment migration from the west than from the east. Published Lu-Hf garnet dates for eclogite-facies metamorphism in the east-central Himalaya as old as -'38-34 Ma may offer a test that the new model fails, because the model predicts that such metamorphism would be restricted to Middle Miocene time. Alternatively, these dates may provide a case study to test suspicions that Lu-Hf garnet dates can exceed actual ages.

## INTRODUCTION

What do we know, and what remains to be discovered, about Himalayan geology? First-order answers are clear: the growth of Earth's highest mountains results from the ongoing collision between the Indian and Eurasian continents. Continuing exploration across a range of geologic length- and time-scales is motivated by many questions, prominently including: (1) What are the initial and boundary conditions, key physical parameters, and idiosyncratic vs. exportable characteristics of mountain-building from this leading natural laboratory for collisional tectonics and continental subduction? (2) In what ways are Himalayan lithospheric processes interacting with atmospheric, biotic, surface, and oceanic processes? and (3) How can we understand and mitigate hazards (e.g., earthquakes, landslides, floods) across these mountains spanning many populous nations?

In this contribution, we first review models for Himalayan tectonics across million-year time-scales. By exploring key data and interpretations, we highlight the need for three dimensional evolutionary models. We then offer an example of such a model: along-strike changes in Himalayan mountain-building could have resulted from the along-strike migration of mid-Cenozoic slab detachment (i.e., slab breakoff). According to this hypothesis, slab evolution and resulting orogenic wedge changes are further speculated to have increased the elevation of the Himalaya and modified the force balance at the plate boundary, in turns yielding (1) increased South Asian monsoon strength through topographic growth, (2) decreased rates of India-Asia convergence by changing the forcing applied to the collisional boundary, and (3) Himalayan asymmetric arc curvature.

## HIMALAYAN TECTONIC MODELS

Long before the plate tectonic revolution, Argand (1924) presciently described the Himalayan Mountains as consequences of the Indian lithosphere underthrusting beneath

Eurasia (**Figure 1A**). Later, plate tectonic models maintained this basic framework (**Figure 1B**) (Dewey and Bird, 1970; Powell and Conaghan, 1973).

In the 1980's, new models were proposed in response to the discovery of the South Tibet fault by Caby et al. (1983) and Burg et al. (1984). The South Tibet fault (also called the South Tibet detachment, and the South Tibet fault system) was first recognized as a north-dipping, top-to-the-north shear zone, and/or a series of closely spaced top-to-the-north faults. This shear zone extends along the crest of the Himalayan Mountains and separates the high-grade crystalline orogenic core to the south from a fold-thrust belt dominated by Paleozoic-Mesozoic Tethyan passive margin strata of northern India to the north (**Figure 2**) (e.g., Burchfiel et al., 1992; Burg et al., 1984; Caby et al., 1983; Herren, 1987). The main characteristics of these South Tibet fault exposures – northerly dip, top-to-the-north shear records, and juxtaposition of lower amphibolite and lesser grade rocks atop upper amphibolite and higher grade rocks – caused it to be quickly interpreted as a normal fault.

The conceptual challenge posed by the early South Tibet fault interpretations – i.e., why would a large normal fault system span the length of Earth's highest contractional mountain chain? – became the focal point of modelling efforts. Many kinematic models envision the South Tibet fault as a normal fault atop an extruding wedge of high grade material (**Figure 1C**). In this context, proposed driving mechanisms for South Tibet fault motion include gravitational sliding along a tilted contact plane (Burg et al., 1984); rotation of principal stresses to near-vertical orientations due to the sharp topographic transition across the Himalayan mountains (Burchfiel and Royden, 1985); subhorizontal shearing below the Himalaya (Yin, 1989); accommodation of the buoyant rise of a partially-subducted upper continental crustal slice, potentially triggered by slab detachment (**Figure 1D**) (Chemenda et al., 1995; Chemenda et al., 2000); and a response to gravitational potential energy changes within the context of critical taper orogen models (e.g., DeCelles et al., 2001; Zhang et al., 2011). Alternately, the South Tibet fault has been interpreted as the upper shear zone atop a channel flow of high-grade material driven southwards by the high gravitational potential of the Tibetan Plateau (**Figure 1E**) (Nelson et al., 1996). Furthermore, such channel rocks may have been extruded to the steep, high topographic front of the range between the South Tibet fault and a basal thrust shear zone (termed the Main Central thrust) as a result of an Early and/or Middle Miocene climate shift that enhanced orographically-focused precipitation and resultant erosional exhumation (**Figure 1E**) (Beaumont et al., 2001; Hodges et al., 2001).

Recognition that the South Tibet fault may be a backthrust led to tectonic wedging models, in which the crystalline core was emplaced at depth (Figure 1F) (Webb et al., 2007; Yin, 2006). Because these models do not include normal faulting, they do not require mechanical considerations beyond contractional boundary conditions.

In light of increasing evidence that the crystalline core of the orogen was built in the Oligocene and Miocene by southwards-propagating thrust stacking (e.g., Ambrose et al., 2015; Carosi et al., 2010; Corrie and Kohn, 2011; Imayama et al., 2010; Montomoli et al., 2013; Reddy et al., 1993), tectonic wedging models have been superseded by duplexing models. Duplexing models posit that the crystalline core of the Himalayan orogen was built via thrust horse accretion, with the South Tibet fault as the active roof backthrust of a middle-to-deep crustal duplex system (**Figure 1G**) (He et al., 2015; Larson et al., 2015).

## KINEMATIC VARIATIONS ALONG THE STRIKE OF THE HIMALAYAN OROGEN

In contrast to the two-dimensional tectonic models, Himalayan geology has significant arc-parallel variability. The South Tibet fault itself – i.e., the central structure of Himalayan tectonic models since the 1980’s – ceases motion at different times along the length of the range (Leloup et al., 2010). This observation is not commonly cited, but can be noted by analysis of existing data. Likewise, patterns of decompression and cooling of the orogen's crystalline core (Warren et al., 2014) indicate variable timing of major processes along strike. Below, we outline these key data sets and discuss their kinematic interpretation.

**South Tibet fault**

South Tibet fault timing data is shown in map view and plotted by longitude against age in Figures 2 and 3, respectively (see also Supplementary Table 1). We show three categories of age data, labeled pre-/syn-motion, post- motion, and $^{40}Ar/^{39}Ar$ muscovite. Pre-/syn-motion data are U-Pb and Th-Pb dates of accessory phase (re-)crystallization (zircon, monazite, etc) in deformed portions of the shear zone. Dated minerals are generally from deformed leucogranites because these are the youngest deformed rocks, and thus provide the tightest constraint on fault motion. Post- motion data also refers to U-Pb and Th-Pb dates of accessory phases, in this case from undeformed leucogranites cross-cutting shear zone fabrics. $^{40}Ar/^{39}Ar$ muscovite ages come from rocks immediately above the shear zone, within the shear zone, and less than 3 km structurally below the shear zone, and ideally record the timing of cooling below an approximate closure temperature of 425 °C (Harrison et al., 2009). Most workers interpret cessation of motion along the sub-horizontal shear zone of the South Tibet fault prior to cooling of the shear zone and its local footwall below this temperature range (e.g., Kellett and Grujic, 2012; cf. Cooper et al., 2013).

Interpretation of pre-/syn-motion age data along the South Tibet fault is straightforward, with the exception of standard geochronological challenges that can impact any dating effort (e.g., Pb-loss and/or metamict damage to zircon). There are two systematic challenges for post-motion ages, and both challenges indicate that these dates might not constrain the termination age of fault motion. First, although the dated leucogranite dikes cross-cut shear zone fabrics, no worker has identified and dated a dike that cross-cuts the entire shear zone of the South Tibet fault. Therefore no one datum can preclude continued motion along the layers of the shear zone that are not cross-cut. Secondly, dated accessory minerals may be inherited (particularly zircon). If so, the crystallization age could pre-date the crystallization of the dike and therefore could pre-date the cessation of shearing along the cross-cut shear zone layers. $^{40}$Ar/$^{39}$Ar muscovite ages are known to suffer from excess Ar across vast swaths of the Himalaya (Herman et al., 2010; Webb et al., 2011), which likewise produces 'excess' ages. Furthermore, robust cooling ages should post-date South Tibet fault motion if the shear zone was sub-horizontal during activity (e.g., Kellett and Grujic, 2012) because observations at nearly all fault localities suggest the deformation temperatures exceeded the temperature range of Ar closure in muscovite. However, if the shear zone was north-dipping during the primary phase of motion (as many workers argue, e.g., Burchfiel et al., 1992), then cooling may coincide with fault motion and these constraints would not constrain cessation of South Tibet fault activity.

Our interpretation of the along-strike variations in South Tibet fault cessation timing is denoted by a grey band in Figure 3b. This band generally traces the younger limit of the pre-/syn-motion ages, because these ages are commonly reliable whereas attempts to date the post-shearing period may regularly yield pre- and/or syn-shearing ages, as discussed above. The interpolation utilizes only post-motion and muscovite ages that are consistent with the younger limits of pre-/syn-motion ages. There are two exceptions: two pre-/syn-motion ages in the east-central Himalaya are sufficiently young relative to the dominant pattern of post-fault motion ages that we assume they are problematic, so we exclude these two ages from the interpolation. The interpreted range of fault cessation timing narrows where data is plentiful (e.g., the central Himalaya), and broadens where there are few published constraints. The interpolated cessation of motion along the South Tibet fault is progressively younger from the western Himalaya (-'24–20 Ma) (e.g., Dézes et al., 1999; Vance et al., 1998) to the east-central Himalaya (-'13-11 Ma) (e.g., Kellett et al., 2009; Wu et al., 1998) (see also

Supplementary Table 1). Less well resolved is a possible reversal in pattern in the easternmost Himalaya, where sparse data show a sharp spatial transition to older ages (~24–20 Ma) at the eastern end of the range (e.g., Yan et al., 2012). Previous workers have speculated that the dominant pattern of eastwards younging in fault cessation timing and a similar pattern in leucogranite crystallization ages may be related to motion along the Karakoram fault (Leech, 2008; Leloup et al., 2010).

The onset of South Tibet fault motion has been speculated to coincide with a metamorphic transition within the Himalayan crystalline core (termed the Greater Himalayan Crystalline duplex in Figure 2) at ca. 27-26 Ma (Figure 3, Supplementary Table 2, e.g., Stübner et al., 2014). Geochemical changes in dated monazite and zircon crystals (e.g., variations through time in heavy rare Earth element concentrations, Rubatto et al., 2013) suggest that the Greater Himalayan Crystalline duplex experienced exclusively prograde metamorphism prior to 27 Ma, whereas after 26 Ma some of these rocks record prograde metamorphism and other parts of this rock package record retrograde metamorphism. Structurally higher rocks record the earliest retrograde metamorphism, and prograde-to-retrograde pressure-temperature paths generally get younger with increasing structural depth within the unit (Corrie and Kohn, 2011; Rubatto et al., 2013). Sparse data suggest that the metamorphic transition occurs at the same time along the strike of the Himalaya (Figure 3b).

**Decompression and cooling of the Himalayan crystalline core**

A synthesis of existing data from sites where multiple pressure conditions have been identified and dated, and from sites where multiple temperature conditions have been identified and dated, allows us to reconstruct decompression-time paths and cooling histories, respectively, along the length of the Himalaya. Such findings from structurally high portions of the Greater Himalayan Crystalline duplex are presented in Figure 3c and d as plots of pressure and temperature vs. time, with the site longitude denoted via color coding (see also

Supplementary Table 3). Furthermore, along-strike cooling patterns are informed via detrital thermochronological dating results from the Himalayan foreland basin compiled in Figure 4 and Supplementary Figure 1 (see also Supplementary Table 4).

Temperature-time constraints from the structurally high portions of the Himalayan crystalline core show that most range sectors cooled from -'750-550 °C at -'26-22 Ma to 200-100 °C by -'15-10 Ma, and that cooling paths varied systematically along the length of the orogen. Specifically, cooling from the highest temperatures through muscovite closure is progressively younger from the western Himalaya to the east-central Himalaya. Sparse pressure-time constraints might be interpreted to match this eastwards younging trend, with the proviso that data of the far eastern Himalaya (from the syntaxial region) do not follow this trend. Instead, these rocks decompressed from -'1.6 GPa at -'24 Ma to -'0.5 GPa at -'17 Ma (Xu et al., 2010). Further aspects of decompression from high pressures across the east-central Himalaya are discussed within the Discussion section, below.

Detrital thermochronology data from foreland basin rocks provide an approximation of the cooling experienced by adjacent Himalayan hinterland regions. A general trend appears in our compilations of $^{40}Ar/^{39}Ar$ muscovite and fission track zircon data: peaks in the cooling age populations appear younger to the east from 25–20 million years ago to 10–8 million years ago (Figure 4 A, B) (e.g., Bernet et al., 2006; Chirouze et al., 2012; Jain et al., 2009; Najman et al., 2003). This is consistent with an eastwards migrating pulse of hinterland cooling during this period. The trend is alternately amplified and diminished by along-strike variations in the depositional ages of samples. For examples, (1) central Himalaya samples deposited before 15 Ma cannot show cooling pulses younger than 15 Ma, and thus visually weight Figure 4A towards older central Himalayan ages, and (2) all zircon fission track samples deposited after 10 Ma are from the central and eastern Himalaya, so all <10 Ma cooling plotted in Figure 4B.i. is visually weighted to these regions. Parsing by 5 million year increments of depositional age helps to see through these visual effects, as in Figure 4B.ii. which highlights zircon fission track samples deposited from 15 to 10 Ma. This plot is consistent with the general suggestion that a cooling pulse migrated eastwards during the Early and Middle Miocene. Further subplots of this type are presented and explored in Supplementary Figure 1, and broadly confirm the trend.

Signals in the Himalayan foreland basin can be complicated by river sediment transport along the range trend, because not all river systems transport sediment perpendicularly away from the mountains and thus might not only represent cooling and exhumation over the limited extent of the range immediately adjacent to the sampling location. Nonetheless, the observed trends of decompression and cooling are roughly synchronous with progressive early and middle Miocene cessation of South Tibet fault motion along the length of the range (Figure 3). As with the South Tibet fault cessation, a pulse of decompression and cooling migrates from the western to the east-central Himalaya. In both cases, sparse data suggest that the easternmost Himalaya features a sharp reversal in this trend.

## 30-8 Ma INDIAN PLATE SUBDUCTION

Because existing Himalayan tectonic models are both two-dimensional and dominantly limited to crustal processes, lithospheric scale processes might help explain the along-strike timing variations noted above. Recent work is promising in this respect, showing that the subducted Indian plate became anchored in the mantle during ongoing collision and then detached from the continental lithosphere via tears that initiated at the ends of the Himalaya and propagated inwards during Late Oligocene-Middle Miocene time (Leary et al., 2016; Replumaz et al., 2010).

India indented Eurasia and moved northwards over the anchored Indian slab from ~30 to ~25 Ma, as evidenced across southern Tibet by a southwards migration of magmatism (DeCelles et al., 2011; Guo et al., 2013) and potentially by the development of the Kailas Basin (Carrapa et al., 2014; DeCelles et al., 2011; Leary et al., 2016) (Figure 2). Detachment of the Indian slab at 25–15 Ma has been interpreted on the bases of (1) metamorphic and melting records indicative of a crustal heating event (Rolland et al., 2001; Stearns et al., 2013) (Supplementary Table 5), (2) changes in patterns of foreland sedimentation, (e.g., Mugnier and Huyghe, 2006) (Supplementary Table 5), and (3) seismic tomographic images of the mantle below India that show a seismically fast region interpreted as detached Indian lithosphere (Replumaz et al., 2010). To explain an eastwards decrease in the distance between the detached slab and the contiguous Indian craton, Replumaz et al. (2010) proposed that detachment of the slab began in the west ca. 25 Ma and migrated to the east-central Himalaya ca. 15 Ma. Similarly, magmatic records from the western to the east-central Himalaya show a west-to-east younging trend, which is consistent with eastward propagation of slab detachment (Guo et al., 2015) (see Figures 2, 3; Supplementary Table 6). For the eastern Himalaya, east-to-west younging of magmatic rocks from ~30–25 Ma at the eastern end to ~15 to 8 Ma in the east-central Himalaya (~90°E) has been interpreted as a product of east-to-west lateral migration of slab detachment (Pan et al., 2012; Zhang et al., 2014) (see Figures 2, 3; Supplementary Table 6).

These findings indicate (i) northward underthrusting of the Indian slab prior to ca. 30 Ma, (ii) slab anchoring and steepening from 30 Ma to 25 Ma, (iii) slab tearing leading to slab detachment initiating at both ends of the Himalaya ca. 25 Ma then migrating towards the central Himalaya, and (iv) final Indian slab break-off occurring in the east-central Himalaya broadly bracketed from 15 to 8 Ma. Intriguingly, the lateral migration of slab detachment along the Himalaya corresponds in time and space with the cessation of motion along the

South Tibet fault and the pulse of cooling and decompression along the Himalayan arc described above.

## A THREE-DIMENSIONAL EVOLUTIONARY MODEL: IMPACTS OF SUBDUCTION DYNAMICS

The spatio-temporal correlation of lateral migration of slab detachment with the Himalayan faulting, decompression, and cooling suggests systematic linkage among these processes. We propose a model in which slab detachment and overall subduction dynamics instigated a series of coupled events, as described in the remainder of this section and detailed in Figures 5 and 6.

### Subduction and Tectonics

In this model, slab anchoring (akin to rollback below the northward advance of India) steepened the sole thrust underlying the Himalaya. Such changes in sole thrust geometry are known to change the mechanical equilibrium and deformation kinematics of the orogenic wedge (Davis et al., 1983). In response to this change, the orogenic wedge thickened and shortened internally, initiating the main development of the Greater Himalayan Crystalline duplex: [1] significant volumes of new material were accreted from the subducting Indian plate not only at the front of the orogenic wedge, but also at depth via duplexing; and [2] the South Tibet fault initiated as a major backthrust, and functioned as the active roof thrust to the underlying duplex. Slab detachment propagated from the ends of the Himalaya towards the east-central Himalaya as the deformation front moved northwards over the anchored slab. As slab detachment propagated, the detached slab portions gradually sank deeper in the mantle and were overridden by the northward-moving Indian continent (Husson et al., 2014; Replumaz et al., 2010). Corresponding southward offset of the vertical traction caused by the weight of the subducted slab rezoned the dynamic deflections of the surface topography

(Husson et al., 2014). Initially, the Indian plate subducted underneath the Himalaya, and the associated dynamic topography maintained the elevation of the Himalaya some 1000-1500 m lower than their plain isostatic elevation. When the subducting slab anchored into the mantle, it moved southward relative to the Indian continent and the Himalaya, which relocated the dynamic deflection further south towards the foreland basin. Corresponding shallowing of the Himalayan sole thrust changed the deformation kinematics of the orogenic wedge once again (à la Dahlen, 1984; Davis et al., 1983), shutting off deep duplexing and backthrusting (see note 12 of Figure 6B). The deep duplexing that thickened the crystalline core persisted for the longest period in the east-central Himalaya (i.e., the region where the final slab detachment occurred), creating a relatively thick crystalline stack there. We interpret the final cessation of South Tibet fault motion in the east-central Himalaya at ~13–11 Ma (Figures 2, 3) as a gross estimate of final slab detachment timing. A contemporaneous extruding wedge system documented across that region, manifested by an out-of-sequence thrust fault below and a steep normal fault above (Kellett and Grujic, 2012), may be a structural response to final slab detachment.

**Dynamic Topography and Monsoon**

Model results suggest that the dynamic deflection over active subducting slabs typically ranges around 1000 m (e.g., Gurnis, 1992; Husson et al., 2012). Husson et al. (2014) states that the increase in elevation accompanying the demise of the slab into the mantle should be on the order of 1 km. Therefore, a topographic rise of this magnitude should start at the two ends of the range (where the horizontal slab tears initiate) at ~25 Ma and migrate from east and west to the east-central Himalaya at 13–11 Ma (Figs. 5, 6).

The high topographic barrier of the Himalaya is a key factor in controlling regional atmospheric flow patterns and thus in generating the South Asian monsoon (Boos and Kuang, 2010). Modeling by Ma et al., (2014) indicates that increases in this topography result in increases of monsoon intensity with a roughly linear relationship. Indeed, multiproxy records of monsoon intensity indicate that the summer monsoon rains were weak prior to ~24 Ma but became progressively stronger up to a peak period from ~15 to 11 Ma (Clift et al., 2008; DeCelles et al., 2007; Sun and Wang, 2005; Tada et al., 2016; Wan et al., 2009). We propose that this temporal correlation between the predicted topographic growth and the monsoon intensity reflects Miocene strengthening of the South Asian monsoon as ultimately a product of subduction dynamics.

**Subduction Dynamics and Convergence**

In each released orogenic region where the sole thrust shallowed after slab detachment, the force balance adjusted accordingly in the Himalayan range. The vertical traction that slab remnants exerted underneath the Himalaya was accompanied by sub-lithospheric shear tractions. These shear tractions contributed to sustain the convergence of India towards Eurasia. When the Indian slab detached, the force switched from a subduction regime where slab pull dominates to a regime where slab suction dominates (Conrad and Lithgow-Bertelloni, 2004). The northward shear force transmitted by the mantle to the Indian plate declined during this transition after the slab detached, and gradually vanished as the slab remnant sank into the mantle. The gradual demise of the Indian slab load as it sinks into the mantle modified the convection pattern and deprived the India-Eurasia convergence of one of its prominent driving forces, and thereby decreased compressive forces at the plate boundary. It follows that convergence rates are predicted to decline during this period. This prediction is broadly consistent with findings from plate circuit reconstructions (e.g., Copley et al., 2010; Iaffaldano et al., 2013; Molnar and Stock, 2009). Such studies show that India-Asia convergence rates quickly dropped after the collision of India ca. 50 Ma and decreased further until ~13–11 Ma, after which convergence rates stabilized or modestly increased. The possibility that slab detachment at ~13-11 Ma produced a change in convergence rates provides an alternative to models in which convergence slowdown results from viscous resistance of intact Tibetan mantle lithosphere (Clark, 2012).

**Slab Detachment and Arc Curvature**

Longitudinal propagation of slab detachment can account for the curvature of the Himalayan mountain belt (see also Capitanio and Replumaz, 2013). The speed of lateral propagation of slab detachment produces variations in orogenic belt curvature: faster propagation produces less curvature and slower propagation produces more curvature. Indentation is faster when it is not lowered by a component of slab pull (which tends to make the trench retreat, whereas indentation makes it advancing), so regions where the longitudinal propagation of slab detachment juxtaposes orogen segments with and without attached slabs are torqued, in a mode similar to retreating subduction zones (Wortel and Spakman, 2000). The degree of bending depends upon the speed of lateral propagation of slab detachment: faster propagation allows less time for regional bending, and thus less arc curvature, and vice versa (Wortel and Spakman, 2000). Because we propose slab detachment propagation across ~2000 km from the west and across ~600 km from the east during the same ~14–12 million year period, our model predicts relatively open arc curvature west of 90°E, and tighter arc curvature to the east of 90°E. Indeed, to the west of 90°E, the Himalaya is renowned for its near-perfect arc, with a ~2000 km radius of curvature (Bendick and Bilham, 2001) (Figure 2). In contrast, farther east the range has tighter curvature (radius of curvature of ~1200 km) (Figure 2).

## DISCUSSION

A variety of data-sets indicate that major phases of Himalayan tectonic development from Late Oligocene through Middle Miocene time occurred asynchronously along the strike of the orogen. Such data include constraints on the cessation of motion along the South Tibet fault, cooling and decompression records, seismic tomography of the detached Indian continental slab, and distribution of volcanic rocks across southern Tibet. These findings show the need for time dependent three-dimensional models. Because most current models are two dimensional, we attempt to create a model including the along-strike dimension. Our model shows major phases of Himalayan construction and uplift controlled by changes in dynamics of the subducting slab. Rollback of the Indian slab relative to the Himalaya initiated development of the Greater Himalayan Crystalline duplex and its roof fault, the South Tibet fault, by altering the balance of forces applied to the orogenic wedge. Lateral migration of slab detachment shut off this structural system progressively along the length of the orogen and released the dynamic deflection of the topography that increased the elevation and strengthened the South Asian monsoon. Simultaneously, the release of dynamic traction from sublithospheric mantle flow after slab detachment may also have been responsible for an observed convergence slowdown.

Below, we first discuss how the slab dynamics model relates to and incorporates aspects of published dimensional models. Next, we explore key issues related to the new model, highlighting: the timing of high-pressure metamorphism in the east-central Himalaya; the state of knowledge of the topography, monsoon, and exhumation across the system; and the post-slab detachment Himalayan development.

**Comparisons of the Slab Dynamics Model to Prior Models**

The model presented in this work is new in that it explores the consequences of the subducting slab evolution for the crustal dynamics of the Himalayan orogenic wedge and South Asian monsoon evolution. However, the modeled lithospheric scale evolution largely follows prior work. Under-thrusting of Eurasia by India is well-established (since the pioneering work of Argand, 1924), and cycles of rollback, lateral migration of slab detachment, and underthrusting with corresponding topographic effects have previously been explored in this region (e.g., Replumaz et al., 2010; DeCelles et al., 2011; Husson et al., 2014; Leary et al., 2016).

The development of the Greater Himalayan Crystalline duplex and the corresponding motion along the South Tibet fault in the new model are generally consistent with the duplexing model presented by He et al. (2015) as well as many aspects of the duplexing model of Larson et al. (2015). As in the duplexing models, the new model shows the development of the Greater Himalayan Crystalline duplex at depth, as a thrust duplex with a roof backthrust (the South Tibet fault) and the slip distance per accreted horse roughly equivalent to horse length (Figure 6). Also similar to the duplexing models and the earlier tectonic wedging models, the slab dynamics model involves late (post-10 Ma) exposure of the main body of the Greater Himalayan Crystalline duplex rocks. This is controversial in that the foreland detrital record is commonly interpreted to indicate Early Miocene erosion of these rocks (e.g., DeCelles et al., 1998). However, prior analyses suggest that such detrital records could be produced by erosion of other Himalayan units in combination with isolated exposures of the Greater Himalayan Crystalline duplex rocks by ~11 Ma (potentially along E-W extensional core complex systems in the Himalayan hinterland) followed by widespread exposure by ~5 Ma (see Yin, 2006 and Webb, 2013).

Incorporation of the slab dynamics history enriches our understanding of proposed duplexing of He et al. (2015) by adding a series of detailed predictions that compare favorably with the geological record. The slab dynamics model offers rationales for why Greater Himalayan Crystalline duplex growth and South Tibet fault motion starts and finishes. Namely, slab anchoring should steepen the Himalayan sole thrust, whereas slab detachment should allow rebound and shallowing of the sole thrust, and such changes to the sole thrust geometry are well understood to start and stop thickening of orogenic wedges (Dahlen, 1984). The model suggests that duplex growth and South Tibet fault motion should initiate after the ~30 Ma start of slab anchoring and before the ~25 Ma start of slab detachment. The ~27-26 Ma metamorphic transition from exclusively prograde to mixed pro- and retro-grade metamorphism (Figure 3, Supplementary Table 2) may signal this onset, with the retrograde metamorphism reflecting exhumation in response to thrust horse stacking. As for cessation timing, the main correlations that led to the model construction are the along-strike correspondence of cooling, decompression, and South Tibet fault cessation with slab detachment migration inferred from seismic tomography and southern Tibetan volcanism.

The slab dynamics model includes a late out-of-sequence extruding wedge system in the east-central Himalaya (Figure 6) that has some commonalities with wedge extrusion models (e.g., Burchfiel and Royden, 1985; Chemenda et al., 1995; 2000). Wedge extrusion occurs as a response to deep burial of light crustal materials and also potentially to slab detachment in the models of Chemenda et al. (1995; 2000). The wedge extrusion of our model is localized to the east-central Himalaya, where a north-dipping brittle normal fault outcropping along the range crest accomplished rapid footwall cooling at ~16 to ~12 Ma (e.g., Carrapa et al., 2016; Kellett et al., 2013), and to the south a contemporaneous out-of-sequence thrust system occurs (e.g., Grujic et al., 2011; Larson et al., 2016). The apparently restricted range of these systems could indicate that they respond to the relatively large magnitude burial and subsequent uplift associated with the final slab detachment, as in the Chemenda group modeling. Localized normal faulting associated with such wedge extrusion can help resolve confusion over South Tibet fault kinematics (i.e., the decade-old debate over whether it is a thrust or a normal fault). In this region (specifically, from eastern Nepal through the Bhutan Himalaya), many exposures of the South Tibet fault along the Himalayan range crest are spatially associated with the north-dipping brittle normal fault (e.g., Carrapa et al., 2016; Kellett et al., 2013). This region hosted much of the early work along the South Tibet fault (e.g., Burg et al., 1984; Burchfiel et al., 1992), and therefore the brittle fault is commonly interpreted as the last phase of South Tibet fault motion. However, this brittle fault is not seen in other sectors of the Himalaya, where structural geometry and cooling histories across the South Tibet fault suggest motion along a sub-horizontal structure (e.g., Vannay et al., 2004; Webb et al., 2013). Sub-horizontal ductile shear dominates South Tibet fault evolution, whereas late brittle normal faulting may cut this shear zone only where a late wedge extrusion system responded to final slab detachment.

**Timing of Eclogite-Facies Metamorphism in the East-Central Himalaya**

The slab dynamics model makes specific claims about the nature and timing of high pressure metamorphism in the east-central Himalaya. Specifically, in the model this metamorphism reflects the steepening and deepening of the orogenic wedge here as the slab steepened. The region would have experienced pressures that were anomalously high, perhaps to eclogite-facies conditions, because it was the last region to experience slab detachment. Deep duplexing and localization of slab weight would have persisted longest here. Also, because the slab was already detached both to east and west of this region prior to final slab detachment, this region would have supported some fraction of the neighboring detached slab weight both to east and west, approximately doubling this effect of excess adjacent weight in the few million years prior to final slab detachment. It follows that the high pressure metamorphism of the lower orogenic wedge should have occurred only in the few million years immediately prior to the ~13-11 Ma final slab detachment. This model prediction is consistent with direct U-Pb dating of zircon in the east-central Himalaya. In combination with geochemical and textural analyses, U-Pb zircon geochronology yields eclogite-facies metamorphic periods of 15.3 ± 0.3 to 14.4 ± 0.3 Ma (Grujic et al., 2011) and 14.9 ± 0.7 to 13.9 ± 1.2 Ma (Wang et al., 2017). However, the model prediction does not appear consistent with (1) published interpretations of Lu-Hf dating of high pressure garnet (Corrie et al., 2010; Kellett et al., 2014) and (2) a study by (Regis et al., 2014) that links monazite geochronology with metamorphism after the high pressure period. These studies argue that high pressure metamorphism in this region occurred as early as ~38 Ma and locally persisted until ~15-13 Ma. Below, we review the latter data sets and their context, show that alternative interpretations are compatible with the slab dynamics model, and discuss broader implications of this analysis.

Isotope geochronology on metamorphic minerals can be used to temporally constrain different parts of the pressure-temperature evolution. For example, Lu-Hf and Sm-Nd geochronology data are commonly interpreted to date early and late stages of metamorphic garnet growth, respectively. This interpretation is based on the fact that garnet preferentially incorporates heavy rare Earth elements (HREE), resulting in high Lu concentration in garnet cores, whereas Sm is rather homogenously distributed (e.g. Kohn, 2009; Lapen et al., 2003). Commonly, growth of garnet can be related to high pressure conditions, and thus application of Lu-Hf garnet geochronology has been used to constrain high pressure metamorphism in the east-central Himalaya at ~26-23 Ma (Corrie et al., 2010), or even as old as ~38-34 Ma (Kellett et al., 2014).

However, recently the interpretation of Lu-Hf age data has been challenged based on evidence for different mechanisms that may modify the extracted age. Skora et al. (2006) presented a model for diffusion-limited uptake of REE in garnet that would create local depletion of the REE around the garnet accompanying the crystal growth and prevent equilibration with the bulk matrix. To the same end, Sousa et al. (2013) used a mass-balance model to show that garnet isotope composition may not equilibrate with the bulk matrix, and thus reactivity and modes of reactant minerals govern the local effective bulk composition and will determine the initial Rb/Sr and/or Lu/Hf during garnet growth. Their modelling suggests significant modification, up to several tens of Ma, in the extracted age for the case of Rb-Sr age data. The case of Lu-Hf is not as straightforward because the source of Lu prior to garnet growth remains elusive and the reactivity of zircon as source of matrix Hf is also unclear. However, a recent study using a large data set of detrital zircons from the Himalaya revealed large variation in the Epsilon-Hf value between -24 to +3, which suggests that zircon may be actively contributing to modification of the matrix composition during metamorphism (Ravikant et al., 2011). Sousa et al. (2013) used this range in Epsilon-Hf values to predict the apparent age error using $^{176}Lu/^{177}Hf$ in garnet. Their calculations indicate that Lu-Hf data may be inaccurate by several Ma years depending on different shifts of the matrix Hf isotope composition caused by zircon recrystallization.

A different mechanism that may alter recorded Lu-Hf ages results from subtle differences in the diffusivity of parent and daughter isotope. Lu diffusion in garnet may be faster than its radiogenic daughter Hf (Mueller et al., 2010; Skora et al., 2006) based on comparison to REE+Hf diffusion data in zircon (Cherniak et al., 1997a; Cherniak et al., 1997b). Recently, this assumption has been also experimentally verified (Bloch et al., 2015). Therefore Lu-Hf is different from other geochronology systems in that its parent isotope, and not the radiogenic daughter, may be preferentially lost from the crystal at sufficiently high temperatures (i.e. above the nominal closure temperature). This may not be problematic if Lu preferentially migrates into (or stays within) the garnet. However, the preferred partitioning of Lu into garnet decreases with increasing temperature, making matrix minerals such as clinopyroxene suitable hosts for Lu (Van Orman et al., 2001). Hence, Lu potentially leaves the garnet at higher rates compared to its radiogenic daughter Hf and may accumulate in grain boundaries (Hiraga et al., 2004) or may be incorporated into matrix minerals or accessory phases. As a result, a lower Lu/Hf ratio is recorded in the garnet that translates into an apparent older age.

These processes may shift the extracted Lu-Hf data towards older ages by as much as tens of millions of years. We therefore interpret previously extracted Lu-Hf data to be potentially modified, and hence high pressure conditions indicated by garnet growth may represent exclusively Middle Miocene metamorphism.

Regis et al. (2014) explore the Jomolhari massif of NW Bhutan and use a different suite of data to argue for eclogitic metamorphism in the east-central Himalaya prior to ~36 Ma. Prior work shows that a mafic eclogite from the northern end of the Jomolhari massif yields a U-Pb titanite cooling age of 14.6 +/- 1.2 Ma (MSWD = 0.2, closure temperature estimated at between ~700 to 500 °C) (Warren et al., 2012). Regis et al. (2014) use monazite petrochronology to show that metasedimentary rocks in the central and southern Jomolhari massif experienced granulite-facies metamorphic conditions of 0.85 GPa and 800 °C at ~36 Ma, and remained at high temperatures until at least ~18 Ma. They use the assumption that the Jomolhari massif represents a coherent rock body to then infer that the high pressure metamorphism (recorded by the mafic eclogite) precedes the granulite-facies metamorphism. In this interpretation, the high pressure metamorphism must be older than ~36 Ma. However, if the Jomolhari massif did not evolve as a coherent rock body, then the northern eclogites may be structurally separated from the southern granulites. For example, the eclogites could be in the hanging wall of an out-of-sequence fault (potentially the Kakhtang thrust of Grujic et al., 2011), and the granulites may be in the footwall. In such cases, eclogitic metamorphism here may have occurred as late as ~17-13 Ma and pre-date structural juxtaposition with the granulitic rocks.

In summary, although prior interpretations of eclogite-facies metamorphism timing across the east-central Himalaya appear inconsistent with the slab dynamics model, viable alternative interpretations of all constraints allow that this metamorphism may have occurred in Middle Miocene time, which is consistent with the model. Of particular interest for geochronological study are the alternative interpretations of Lu-Hf garnet dates, which suggest that these dates are not accurate in that they are much older than the actual timing of the eclogite facies metamorphism. Further exploration of the prograde-to-peak metamorphic timing here may confirm long-standing hypotheses that Lu-Hf garnet dates could greatly exceed the geological ages of dated events (e.g., Skora et al., 2006).

**Monsoon vs. Mountain Building**

Construction of mountain chains and elevated plateaus is understood to be strongly influenced by climate-modulated erosion (Beaumont et al., 2001; Konstantinovskaia and Malavieille, 2005; Montgomery et al., 2001), and by subducting plate (or ‘slab’) dynamics (Carrapa et al., 2014; Fox et al., 2015; Replumaz et al., 2010; Wortel and Spakman, 2000). However, how climate and slab dynamics impact each other during mountain building remains poorly understood (Iaffaldano et al., 2011; Lamb and Davis, 2003). Various chicken-vs-egg interpretative challenges further limit our ability to decipher climate-erosion-tectonics interactions (Clift et al., 2008; Molnar and England, 1990). For instance, for many mountain belts it is unclear whether tectonic shifts forced climatic changes, or climatic shifts generated new tectonic regimes. These issues are well-illustrated in studies of the Himalaya, where subduction dynamics is recognized to uplift the range (Husson et al., 2014) and deform the Tibetan Plateau (DeCelles et al., 2011; Replumaz et al., 2014), but models of the kinematic evolution of the Himalayan mountains feature static subduction zone geometries (e.g., Beaumont et al., 2001; Herman et al., 2010; Webb, 2013) with only few exceptions (Carrapa et al., 2014; King et al., 2011). The rise of the Himalayan mountains is thought to explain the development of the South Asian monsoon (Boos and Kuang, 2010), yet the only published model with a significant role for climate – the channel flow model – shows major rock uplift and exhumation as triggered by enhanced erosion resulting from the onset of the monsoon (Beaumont et al., 2001; Clift et al., 2008). The new model suggests instead that slab dynamics triggered a phase of Himalayan uplift, which in turn caused the intensification of the South Asian monsoon. Therefore, because subduction dynamics remains a priori unaffected by climate vagaries, the problem is in principle no longer a chicken-and-egg issue, but instead has a univocal relationship. There is a trigger and a target. Nevertheless, climate-induced erosion can modulate mantle convection and therefore tectonic velocities (Iaffaldano et al., 2011), so if future work can demonstrate that slab anchoring and detachment may be induced by climatic changes then the feedback loop will close again.

**Post-Slab Detachment Tectonics**

In the context of the slab dynamics model, slab detachment would produce a shallowing of the Himalayan sole thrust, a maximum of topography, and arc curvature (Figures 5, 6). We speculate that these factors could have had a broad range of consequences for post-slab detachment tectonics:

The high topography might have created a positive feedback between climate and tectonics, thereby maintaining the high topography. This could have worked as follows: by intensifying the monsoon, erosion increased, leading to structural changes making shallow-to-mid crustal duplexing more vertically-directed (i.e., antiformal stack development, a la Konstantinovskaia and Malavieille, 2005), thereby providing the uplift necessary to maintain high topography and, in turn, the strong monsoon.

Normal fault systems accomplishing orogen-parallel extension across the northern Himalaya are thought to result from orogen-perpendicular thrusting along the Himalayan arc, because as rock packages are thrust forward they must span arc segments of increasing length (Murphy et al., 2009). If arc curvature does control these systems, then proposed progressive development of arc curvature in response to the lateral migration of slab detachment would predict that these systems initiated at different times along the length of the arc. Sparse data support this possibility, as the Leo Pargil extensional system of the western Himalaya may have developed at ~23 Ma, some ~8 million years prior to the development of similar systems in the east-central Himalaya (Langille et al., 2012).

Finally, a series of papers have coupled thermochronological data with balanced palinspastic reconstructions to argue for variations in Himalayan shortening rates of up to an order of magnitude over the last ~20 million years (Long et al., 2012; McQuarrie and Ehlers, 2015; Robinson and McQuarrie, 2012; Tobgay et al., 2012). These reconstructions have not considered slab dynamics impacts on the crustal kinematics and cooling histories. The along-strike temporal correlation between cooling pulses and slab detachment suggests that these reconstructions would benefit from re-evaluation.

## CONCLUSIONS AND BROAD CONSIDERATIONS

Many explorations of Himalayan tectonics in recent years have focused on along-strike changes in tectonic processes, and these focus almost entirely on post-Miocene processes (e.g., Cannon and Murphy, 2014; Copeland et al., 2015; Grujic et al., 2006; van der Beek et al., 2016). In this work we show along-strike timing variations in Oligocene-Miocene Himalayan tectonic processes, and relate these to a model in which the deformation of the Himalayan orogenic wedge was largely governed by slab dynamics processes. The model suggests that the along-strike timing variations were controlled by lateral migration of slab-detachment. Some exciting outcomes of the model are new explanations for the intensification of the South Asian monsoon, the Miocene slowdown of India-Eurasia convergence, and the development of asymmetric Himalayan arc curvature.

The proposed slab dynamics model also changes our understanding of Miocene Himalayan development within the broader context of East Asian collisional tectonics. Slab detachment is thought to initiate motion on major strike-slip faults within East Asia (Replumaz et al., 2014), suggesting that strong links between collision frontal and intracontinental deformation are controlled by slab dynamics. Finally, recognition of climatic-tectonic links during Miocene slab detachment may be combined with knowledge of earlier slab anchoring-detachment-underthrusting cycles along Asia's southern margin (DeCelles et al., 2011; Husson et al., 2014; Kapp et al., 2007; Replumaz et al., 2010) and elsewhere to explore how slab dynamics may have modulated climate throughout Earth's plate tectonic history.

Thus far, community responses as we attempt to introduce this work have focused on the question of whether the model is "right" or not. To the reader, we recommend that it is more important to check for present viability, since all models eventually meet Ozymandian fates. Further, it is yet more important to consider whether the compiled data truly require significant third-dimensional variability during the Oligocene-Miocene development of the Himalayan Mountains. If so, then the present model serves as an early attempt to grapple with this variability, and we anticipate better works in the future.

## ACKNOWLEDGMENTS

We thank Fabio A. Capitanio and two anonymous reviewers for feedback on a closely-related, rejected manuscript; they helped inform our approach to this work. Reviews from J. Matthew Cannon and two anonymous reviewers helped us clarify the present contribution. Discussions with Jason Ali, Jess King, and Ryan McKenzie helped us clarify our concepts and communication. Funding for this work comes from the US National Science Foundation (EAR-1322033 to A.A.G. Webb) and the Chinese Natural Science Foundation (grant 41430212 to Z. Xu, H. Cao, Q. Wang, and A.A.G. Webb). AAGW dedicates this work to XC.

**REFERENCES CITED**


Aitchison, J., Davis, A., Badengzhu, B., Luo, H., 2002. New constraints on the India–Asia collision: the Lower Miocene Gangrinboche conglomerates, Yarlung Tsangpo suture zone, SE Tibet. Journal of Asian Earth Sciences 21.

Aitchison, J.C., Ali, J.R., Davis, A.M., 2007. When and where did India and Asia collide? Journal of Geophysical Research 112.

Ambrose, T.K., Larson, K.P., Guilmette, C., Cottle, J.M., Buckingham, H., Rai, S., 2015. Lateral extrusion, underplating, and out-of-sequence thrusting within the Himalayan metamorphic core, Kanchenjunga, Nepal. Lithosphere 7, 441-464.

An, W., Hu, X., Garzanti, E., BouDagher-Fadel, M.K., Wang, J., Sun, G., 2014. Xigaze forearc basin revisited (South Tibet): Provenance changes and origin of the Xigaze Ophiolite. Geological Society of America Bulletin 126.

Argand, E., 1924. La Tectonique de l'Asia. Extrait du Compte-rendu du XIIIe Congrès géologique international 1922 (Liège) 1(5), 171-372.

Beaumont, C., Jamieson, R.A., Nguyen, M.H., Lee, B., 2001. Himalayan tectonics explained by extrusion of a low-viscosity crustal channel coupled to focused surface denudation. Nature 414, 738-742.

Bendick, R., Bilham, R., 2001. How perfect is the Himalayan arc? Geology 29, 791-794.

Bernet, M., Garver, J.I., 2005. Fission-track analysis of detrital zircon. Reviews in Mineralogy & Geochemistry 58.

Bernet, M., van der Beek, P., Pik, R., Huyghe, P., Mugnier, J.-L., Labrin, E., and Szulc, A., 2006, Miocene to Recent exhumation of the central Himalaya determined from combined detrital zircon fission-track and U/Pb analysis of Siwalik sediments, western Nepal: Basin Research, v. 18, no. 4.

Bloch, E., Ganguly, J., Hervig, R., Cheng, W., 2015. 176Lu–176Hf geochronology of garnet I: experimental determination of the diffusion kinetics of Lu3+ and Hf4+ in garnet, closure temperatures and geochronological implications. Contributions to Mineralogy and Petrology 169.

Boos, W.R., Kuang, Z., 2010. Dominant control of the South Asian monsoon by orographic insulation versus plateau heating. Nature 463, 218-222.

Burchfiel, B.C., Chen, Z., Hodges, K.V., Liu, Y., Royden, L.H., Deng, C., Xu, J., 1992. The South Tibetan Detachment System, Himalayan Orogen: Extension contemporaneous with and parallel to shortening in a collisional mountain belt. Geol. Soc. Am. Spec. Paper 269.

Burchfiel, B.C., Royden, L.H., 1985. North-south extension within the convergent Himalayan region. Geology 13.

Burg, J.P., Brunel, M., Gapais, D., Chen, G.M., Liu, G.H., 1984. Deformation of leucogranites of the crystalline Main Central Sheet in southern Tibet (China). Journal of Structural Geology 6, 535-542.

Caby, R., Pecher, A., Le Fort, P., 1983. Le grand chevauchement central himalayen: nouvelles donnees sur le metamorphisme inverse a la base de la Dalle du Tibet. Revue de geologie dynamique et de geographie physique 24, 89-100.

Cannon, J. M., and Murphy, M. A., 2014, Active lower crustal deformation and Himalayan seismic hazard revealed by stream channels and regional geology: Tectonophysics, v. 633, p. 34-42.

Capitanio, F.A., Replumaz, A., 2013. Subduction and slab breakoff controls on Asian indentation tectonics and Himalayan western syntaxis formation. Geochemistry Geophysics Geosystems 14, 3515-3531.

Capitanio, F.A., Replumaz, A., Riel, N., 2015. Reconciling subduction dynamics during Tethys closure with large-scale Asian tectonics: Insights from numerical modeling. Geochemistry, Geophysics, Geosystems 16.

Carosi, R., Montomoli, C., Rubatto, D., Visonà, D., 2010. Late Oligocene high-temperature shear zones in the core of the Higher Himalayan Crystallines (Lower Dolpo, western Nepal). Tectonics 29.

Carrapa, B., Orme, D.A., DeCelles, P.G., Kapp, P., Cosca, M.A., Waldrip, R., 2014. Miocene burial and exhumation of the India-Asia collision zone in southern Tibet: Response to slab dynamics and erosion. Geology 42, 443-446.

Carrapa, B., Robert, X., DeCelles, P.G., Orme, D.A., Thomson, S.N., Schoenbohm, L.M., 2016. Asymmetric exhumation of the Mount Everest region: Implications for the tectono-topographic evolution of the Himalaya. Geology 44, 611-614.

Chemenda, A., Mattauer, M., Malavieille, J., Bokun, A., 1995. A mechanism for syn-collisional rock exhumation and associated normal faulting: Results from physical modelling. Earth and Planetary Science Letters 132.

Chemenda, A.I., Burg, J.-P., Mattauer, M., 2000. Evolutionary model of the Himalaya–Tibet system: geopoem based on new modelling, geological and geophysical data. Earth and Planetary Science Letters 174.

Cherniak, D., Hanchar, J., Watson, E., 1997a. Diffusion of tetravalent cations in zircon. Contributions to Mineralogy and Petrology 127.

Cherniak, D.J., Hanchar, J.M., Watson, E.B., 1997b. Rare-earth diffusion in zircon. Chemical Geology 134.

Chirouze, F., Bernet, M., Huyghe, P., Erens, V., Dupont-Nivet, G., and Senebier, F., 2012, Detrital thermochronology and sediment petrology of the middle Siwaliks along the

Muksar Khola section in eastern Nepal: Journal of Asian Earth Sciences, v. 44, p. 117-135.

Clark, M. K., 2012, Continental collision slowing due to viscous mantle lithosphere rather than topography: Nature, v. 483, no. 7387, p. 74-77.

Clift, P., Hodges, K., Heslop, D., Hannigan, R., Long, H., Calves, G., 2008. Correlation of Himalayan exhumation rates and Asian monsoon intensity. Nature Geoscience 1.

Conrad, C.P., Lithgow-Bertelloni, C., 2004. The temporal evolution of plate driving forces: Importance of "slab suction" versus "slab pull" during the Cenozoic. Journal of Geophysical Research-Solid Earth 109.

Cooper, F.J., Hodges, K.V., Adams, B.A., 2013. Metamorphic constraints on the character and displacement of the South Tibetan fault system, central Bhutanese Himalaya. Lithosphere 5, 67-81.

Copeland, P., Bertrand, G., France-Lanord, C., and Sundell, K., 2015, Ar-40/Ar-39 ages of muscovites from modern Himalayan rivers: Himalayan evolution and the relative contribution of tectonics and climate: Geosphere, v. 11, no. 6, p. 1837-1859.

Copley, A., Avouac, J.P., Royer, J.Y., 2010. India-Asia collision and the Cenozoic slowdown of the Indian plate: Implications for the forces driving plate motions. Journal of Geophysical Research: Solid Earth (1978–2012) 115.

Corrie, S.L., Kohn, M.J., 2011. Metamorphic history of the central Himalaya, Annapurna region, Nepal, and implications for tectonic models. Geological Society of America Bulletin 123.

Corrie, S.L., Kohn, M.J., Vervoort, J.D., 2010. Young eclogite from the Greater Himalayan Sequence, Arun Valley, eastern Nepal: P–T–t path and tectonic implications. Earth and Planetary Science Letters 289.

Dahlen, F.A., 1984. Noncohesive Critical Coulomb Wedges - an Exact Solution. Journal of Geophysical Research 89, 125-133.

Davis, D., Suppe, J., Dahlen, F.A., 1983. Mechanics of fold-and-thrust belts and accretionary wedges. Journal of Geophysical Research 88.

DeCelles, P.G., Kapp, P., Quade, J., Gehrels, G.E., 2011. Oligocene-Miocene Kailas basin, southwestern Tibet: Record of postcollisional upper-plate extension in the Indus-Yarlung suture zone. Geological Society of America Bulletin 123.

DeCelles, P.G., Quade, J., Kapp, P., Fan, M.J., Dettman, D.L., Ding, L., 2007. High and dry in central Tibet during the Late Oligocene. Earth and Planetary Science Letters 253, 389-401.

DeCelles, P.G., Robinson, D.M., Quade, J., Ojha, T.P., Garzione, C.N., Copeland, P., Upreti, B.N., 2001. Stratigraphy, structure, and tectonic evolution of the Himalayan fold-thrust belt in western Nepal. Tectonics 20.

DeCelles, P. G., Gehrels, G. E., Quade, J., Ojha, T. P., Kapp, P. A., and Upreti, B. N., 1998, Neogene foreland basin deposits, erosional unroofing, and the kinematic history of the Himalayan fold-thrust belt, western Nepal: Geological Society of America Bulletin, v. 110, no. 1, p. 2-21.

Dewey, J.F., Bird, J.M., 1970. Mountain belts and the new global tectonics. Journal of Geophysical Research 75, 2625-2647.

Dézes, P., Vannay, J. C., Steck, A., Bussy, F., and Cosca, M., 1999, Synorogenic extension: Quantitative constraints on the age and displacement of the Zanskar shear zone (northwest Himalaya): Geological Society of America Bulletin, v. 111, no. 3, p.364-374.

Ding, L., Kapp, P., Wan, X., 2005. Paleocene–Eocene record of ophiolite obduction and initial India-Asia collision, south central Tibet. Tectonics 24.

England, P., and Houseman, G., 1986, Finite Strain Calculations of Continental Deformation .2. Comparison with the India-Asia Collision Zone: Journal of Geophysical Research-Solid Earth and Planets, v. 91, no. B3, p. 3664-3676.

Fox, M., Herman, F., Kissling, E., Willett, S.D., 2015. Rapid exhumation in the Western Alps driven by slab detachment and glacial erosion. Geology 43, 379-382.

Greenwood, L.V., Argles, T.W., Parrish, R.R., Harris, N.B.W., Warren, C., 2016. The geology and tectonics of central Bhutan. Journal of the Geological Society 173.

Grujic, D., Coutand, I., Bookhagen, B., Bonnet, S., Blythe, A., and Duncan, C., 2006, Climatic forcing of erosion, landscape, and tectonics in the Bhutan Himalayas: Geology, v. 34, no. 10, p. 801-804.

Grujic, D., Warren, C.J., Wooden, J.L., 2011. Rapid synconvergent exhumation of Miocene-aged lower orogenic crust in the eastern Himalaya. Lithosphere 3, 346-366.

Guo, Z., Wilson, M., Zhang, M., Cheng, Z., Zhang, L., 2013. Post-collisional, K-rich mafic magmatism in south Tibet: constraints on Indian slab-to-wedge transport processes and plateau uplift. Contributions to Mineralogy and Petrology 165.

Guo, Z., Wilson, M., Zhang, M., Cheng, Z., Zhang, L., 2015. Post-collisional Ultrapotassic Mafic Magmatism in South Tibet: Products of Partial Melting of Pyroxenite in the Mantle Wedge Induced by Roll-back and Delamination of the Subducted Indian Continental Lithosphere Slab. Journal of Petrology 56.

Gurnis, M., 1992. Rapid Continental Subsidence Following the Initiation and Evolution of Subduction. Science 255, 1556-1558.

Harrison, T., Célérier, J., Aikman, A., Hermann, J., Heizler, M., 2009. Diffusion of 40Ar in muscovite. Geochimica et Cosmochimica Acta 73.

He, D., Webb, A.A.G., Larson, K.P., Martin, A.J., Schmitt, A.K., 2015. Extrusion vs. duplexing models of Himalayan mountain building 3: duplexing dominates from the Oligocene to Present. International Geology Review 57.

He, D., Webb, A.A.G., Larson, K.P., Schmitt, A.K., 2016. Extrusion vs. duplexing models of Himalayan mountain building 2: The South Tibet detachment at the Dadeldhura klippe. Tectonophysics 667, 87-107.

Henderson, A.L., Najman, Y., Parrish, R., Mark, D.F., Foster, G.L., 2011. Constraints to the timing of India–Eurasia collision; a re-evaluation of evidence from the Indus Basin sedimentary rocks of the Indus–Tsangpo Suture Zone, Ladakh, India. Earth-Science Reviews 106.

Herman, F., Copeland, P., Avouac, J.-P., Bollinger, L., Mahéo, G., Fort, P., Rai, S., Foster, D., Pêcher, A., Stüwe, K., Henry, P., 2010. Exhumation, crustal deformation, and thermal structure of the Nepal Himalaya derived from the inversion of thermochronological and thermobarometric data and modeling of the topography. Journal of Geophysical Research 115.

Herren, E., 1987. Zanskar shear zone: Northeast-southwest extension within the Higher Himalayas (Ladakh, India). Geology 15, 409-413.

Hiraga, T., Anderson, I.M., Kohlstedt, D.L., 2004. Grain boundaries as reservoirs of incompatible elements in the Earth's mantle. Nature 427, 699-703.

Hodges, K.V., Hurtado, J.M., Whipple, K.X., 2001. Southward extrusion of Tibetan crust and its effect on Himalayan tectonics. Tectonics 20.

Husson, L., Bernet, M., Guillot, S., Huyghe, P., Mugnier, J.-L., Replumaz, A., Robert, X., Beek, P.V.d., 2014. Dynamic ups and downs of the Himalaya. Geology 42, 839-842.

Husson, L., Guillaume, B., Funiciello, F., Faccenna, C., Royden, L.H., 2012. Unraveling topography around subduction zones from laboratory models. Tectonophysics 526, 5-15.

Iaffaldano, G., Bodin, T., and Sambridge, M., 2013, Slow-downs and speed-ups of India-Eurasia convergence since similar to 20 Ma: Data-noise, uncertainties and dynamic implications: Earth and Planetary Science Letters, v. 367, p. 146-156.

Iaffaldano, G., Husson, L., Bunge, H.-P., 2011. Monsoon speeds up Indian plate motion. Earth and Planetary Science Letters 304.

Imayama, T., Takeshita, T., Arita, K., 2010. Metamorphic P-T profile and P-T path discontinuity across the far-eastern Nepal Himalaya: investigation of channel flow models. Journal of Metamorphic Geology 28, 527-549.

Jain, A. K., Lal, N., Sulemani, B., Awasthi, A. K., Singh, S., Kumar, R., and Kumar, D., 2009, Detrital-zircon fission-track ages from the Lower Cenozoic sediments, NW Himalayan foreland basin: Clues for exhumation and denudation of the Himalaya during the India-Asia collision: Geological Society of America Bulletin, v. 121, no. 3-4, p. 519-535.

Kapp, P., DeCelles, P.G., Gehrels, G.E., Heizler, M., Ding, L., 2007. Geological records of the Lhasa-Qiangtang and Indo-Asian collisions in the Nima area of central Tibet. Geological Society of America Bulletin 119.

Kellett, D.A., Cottle, J.M., Smit, M., 2014. Eocene deep crust at Ama Drime, Tibet: Early evolution of the Himalayan orogen. Lithosphere 6, 220-229.

Kellett, D.A., Grujic, D., 2012. New insight into the South Tibetan detachment system: Not a single progressive deformation. Tectonics 31.

Kellett, D.A., Grujic, D., Coutand, I., Cottle, J., Mukul, M., 2013. The South Tibetan detachment system facilitates ultra rapid cooling of granulite-facies rocks in Sikkim Himalaya. Tectonics 32.

Kellett, D. A., Grujic, D., and Erdmann, S., 2009, Miocene structural reorganization of the South Tibetan detachment, eastern Himalaya: Implications for continental collision: Lithosphere, v. 1, no. 5, p. 259-281.

King, J., Harris, N., Argles, T., Parrish, R., Zhang, H., 2011. Contribution of crustal anatexis to the tectonic evolution of Indian crust beneath southern Tibet. Geological Society of America Bulletin 123.

Kohn, M., 2009. Models of garnet differential geochronology. Geochimica et Cosmochimica Acta 73.

Konstantinovskaia, E., Malavieille, J., 2005. Erosion and exhumation in accretionary orogens: Experimental and geological approaches. Geochemistry, Geophysics, Geosystems 6.

Lamb, S., Davis, P., 2003. Cenozoic climate change as a possible cause for the rise of the Andes. Nature 425, 792-797.

Langille, J.M., Jessup, M.J., Cottle, J.M., Lederer, G., Ahmad, T., 2012. Timing of metamorphism, melting and exhumation of the Leo Pargil dome, northwest India. Journal of Metamorphic Geology 30.

Lapen, T., Johnson, C., Baumgartner, L., Mahlen, N., Beard, B., Amato, J., 2003. Burial rates during prograde metamorphism of an ultra-high-pressure terrane: an example from Lago di Cignana, western Alps, Italy. Earth and Planetary Science Letters 215.

Larson, K., Ambrose, T., Webb, A., Cottle, J., Shrestha, S., 2015. Reconciling Himalayan midcrustal discontinuities: The Main Central thrust system. Earth and Planetary Science Letters 429.

Larson, K.P., Kellett, D.A., Cottle, J.M., King, J., Lederer, G., Rai, S.M., 2016. Anatexis, cooling, and kinematics during orogenesis: Miocene development of the Himalayan metamorphic core, east-central Nepal. Geosphere 12, 1575-1593.

Leary, R., Orme, D.A., Laskowski, A.K., DeCelles, P.G., Kapp, P., Carrapa, B., Dettinger, M., 2016. Along-strike diachroneity in deposition of the Kailas Formation in central southern Tibet: Implications for Indian slab dynamics. Geosphere 12, 1198-1223.

Leech, M.L., 2008. Does the Karakoram fault interrupt mid-crustal channel flow in the western Himalaya? Earth and Planetary Science Letters 276, 314-322.

Leloup, P.H., Mahéo, G., Arnaud, N., Kali, E., Boutonnet, E., Liu, D., Xiaohan, L., Haibing, L., 2010. The South Tibet detachment shear zone in the Dinggye area Time constraints on extrusion models of the Himalayas. Earth and Planetary Science Letters 292.

Long, S.P., McQuarrie, N., Tobgay, T., Coutand, I., Cooper, F.J., Reiners, P.W., Wartho, J.A., Hodges, K.V., 2012. Variable shortening rates in the eastern Himalayan thrust belt, Bhutan: Insights from multiple thermochronologic and geochronologic data sets tied to kinematic reconstructions. Tectonics 31.

Ma, D., Boos, W., Kuang, Z., 2014. Effects of orography and surface heat fluxes on the South Asian summer monsoon. Journal of Climate 27, 6647-6659.

McQuarrie, N., Ehlers, T.A., 2015. Influence of thrust belt geometry and shortening rate on thermochronometer cooling ages: Insights from thermokinematic and erosion modeling of the Bhutan Himalaya. Tectonics 34, 1055-1079.

Molnar, P., England, P., 1990. Late Cenozoic uplift of mountain ranges and global climate change: chicken or egg? Nature 346.

Molnar, P., Stock, J.M., 2009. Slowing of India's convergence with Eurasia since 20 Ma and its implications for Tibetan mantle dynamics. Tectonics 28.

Montgomery, D.R., Balco, G., Willett, S.D., 2001. Climate, tectonics, and the morphology of the Andes. Geology 29.

Montomoli, C., Iaccarino, S., Carosi, R., Langone, A., Visonà, D., 2013. Tectonometamorphic discontinuities within the Greater Himalayan Sequence in Western

Nepal (Central Himalaya): Insights on the exhumation of crystalline rocks. Tectonophysics 608, 1349-1370.

Mueller, T., Watson, E.B., Harrison, T.M., 2010. Applications of Diffusion Data to High-Temperature Earth Systems. Diffusion in Minerals and Melts 72, 997-1038.

Mugnier, J.-L., Huyghe, P., 2006. Ganges basin geometry records a pre-15 Ma isostatic rebound of Himalaya. Geology 34, 445-448.

Najman, Y., Garzanti, E., Pringle, M., Bickle, M., Stix, J., and Khan, I., 2003, Early-Middle Miocene paleodrainage and tectonics in the Pakistan Himalaya: Geological Society of America Bulletin, v. 115, no. 10, p. 1265-1277.

Nelson, K.D., Zhao, Brown, L.D., Kuo, Che, Liu, Klemperer, S.L., Makovsky, Meissner, Mechie, Kind, Wenzel, Ni, Nabelek, Leshou, Tan, Wei, Jones, A.G., Booker, Unsworth, Kidd, W.S.F., Hauck, Alsdorf, Ross, Cogan, Wu, Sandvol, Edwards, 1996. Partially Molten Middle Crust Beneath Southern Tibet: Synthesis of Project INDEPTH Results. Science (New York, N.Y.) 274, 1684-1688.

Pan, F.-B., Zhang, H.-F., Harris, N., Xu, W.-C., Guo, L., 2012. Oligocene magmatism in the eastern margin of the east Himalayan syntaxis and its implication for the India–Asia post-collisional process. Lithos 154, 181-192.

Pan, G.T., Ding, J., Yao, D.S., Wang, L.Q., 2004. Geological map of the Qinghai-Xizang (Tibet) Plateau and adjacent areas. Chengdu, Chengdu Cartographic Publishing House, scale: 1:1,000,000.

Peltzer, G., and Tapponnier, P., 1988, Formation and Evolution of Strike-Slip Faults, Rifts, and Basins during the India-Asia Collision - an Experimental Approach: Journal of Geophysical Research-Solid Earth and Planets, v. 93, no. B12, p. 15085-15117.

Powell, C., Conaghan, P.J., 1973. Plate tectonics and the Himalayas. Earth and Planetary Science Letters 20, 1-12.

Ravikant, V., Wu, F.-Y., Ji, W.-Q., 2011. U–Pb age and Hf isotopic constraints of detrital zircons from the Himalayan foreland Subathu sub-basin on the Tertiary palaeogeography of the Himalaya. Earth and Planetary Science Letters 304.

Reddy, S.M., Searle, M.P., Massey, J.A., 1993. Structural evolution of the High Himalayan Gneiss sequence, Langtang valley, Nepal, In: Treloar, P.J., Searle, M.P. (Eds.), Himalayan Tectonics. Geological Society of London, London, pp. 375-389.

Regis, D., Warren, C.J., Young, D., Roberts, N.M.W., 2014. Tectono-metamorphic evolution of the Jomolhari massif: Variations in timing of syn-collisional metamorphism across western Bhutan. Lithos 190-191, 449-466.

Replumaz, A., Capitanio, F., Guillot, S., Negredo, A.M., Villaseñor, A., 2014. The coupling of Indian subduction and Asian continental tectonics. Gondwana Research 26.

Replumaz, A., Negredo, A.M., Villaseñor, A., Guillot, S., 2010. Indian continental subduction and slab break-off during Tertiary collision. Terra Nova 22, 290-296.

Robinson, D.M., McQuarrie, N., 2012. Pulsed deformation and variable slip rates within the central Himalayan thrust belt. Lithosphere 4, 449-464.

Rohrmann, A., Kapp, P., Carrapa, B., Reiners, P.W., Guynn, J., Ding, L., Heizler, M., 2012. Thermochronologic evidence for plateau formation in central Tibet by 45 Ma. Geology 40, 187-190.

Rolland, Y., Mahéo, G., Guillot, S., Pecher, A., 2001. Tectono-metamorphic evolution of the Karakoram Metamorphic complex (Dassu-Askole area, NE Pakistan): exhumation of mid-crustal HT-MP gneisses in a convergent context. Journal of Metamorphic Geology 19.

Rubatto, D., Chakraborty, S., Dasgupta, S., 2013. Timescales of crustal melting in the Higher Himalayan Crystallines (Sikkim, Eastern Himalaya) inferred from trace element-constrained monazite and zircon chronology. Contributions to Mineralogy and Petrology 165, 349-372.

Skora, S., Baumgartner, L., Mahlen, N., Johnson, C., Pilet, S., Hellebrand, E., 2006. Diffusion-limited REE uptake by eclogite garnets and its consequences for Lu–Hf and Sm–Nd geochronology. Contributions to Mineralogy and Petrology 152.

Sousa, J., Kohn, M., Schmitz, M., Northrup, C., Spear, F., 2013. Strontium isotope zoning in garnet: implications for metamorphic matrix equilibration, geochronology and phase equilibrium modelling. Journal of Metamorphic Geology 31.

Stearns, M.A., Hacker, B.R., Ratschbacher, L., Lee, J., Cottle, J.M., Kylander-Clark, A., 2013. Synchronous Oligocene–Miocene metamorphism of the Pamir and the north Himalaya driven by plate-scale dynamics. Geology 41, 1071-1074.

Stübner, K., Grujic, D., Parrish, R.R., Roberts, N.M.W., Kronz, A., Wooden, J., Ahmad, T., 2014. Monazite geochronology unravels the timing of crustal thickening in NW Himalaya. Lithos 210-211, 111-128.

Sun, X.J., Wang, P.X., 2005. How old is the Asian monsoon system? Palaeobotanical records from China. Palaeogeography Palaeoclimatology Palaeoecology 222, 181-222.

Tada, R., Zheng, H., Clift, P., 2016. Evolution and variability of the Asian monsoon and its potential linkage with uplift of the Himalaya and Tibetan Plateau. Progress in Earth and Planetary Science 3, 1-26.

Thakur, V.C., Rawat, B.S., 1992. Geological map of the Western Himalaya. Dehra Dun, Wadia Institute of Himalayan Geology, scale: 1:1,000,000.

Tobgay, T., McQuarrie, N., Long, S., Kohn, M., Corrie, S., 2012. The age and rate of displacement along the Main Central Thrust in the western Bhutan Himalaya. Earth and Planetary Science Letters 319.

van der Beek, P., Litty, C., Baudin, M., Mercier, J., Robert, X., and Hardwick, E., 2016, Contrasting tectonically driven exhumation and incision patterns, western versus central Nepal Himalaya: Geology, v. 44, no. 4, p. 327-330.

Van Orman, J.A., Grove, T.L., Shimizu, N., 2001. Rare earth element diffusion in diopside: influence of temperature, pressure, and ionic radius, and an elastic model for diffusion in silicates. Contributions to Mineralogy and Petrology 141.

Vance, D., Ayres, M., Kelley, S., and Harris, N., 1998, The thermal response of a metamorphic belt to extension: constraints from laser Ar data on metamorphic micas: Earth and Planetary Science Letters, v. 162, no. 1-4, p. 153-164.

Vannay, J.-C., Grasemann, B., Rahn, M., Frank, W., Carter, A., Baudraz, V., Cosca, M., 2004. Miocene to Holocene exhumation of metamorphic crustal wedges in the NW Himalaya: Evidence for tectonic extrusion coupled to fluvial erosion. Tectonics 23.

Vannay, J.C., Grasemann, B., 1998. Inverted metamorphism in the High Himalaya of Himachal Pradesh (NW India): phase equilibria versus thermobarometry. Schweizerische Mineralogische Und Petrographische Mitteilungen 78.

Vermeesch, P., 2004. How many grains are needed for a provenance study? Earth and Planetary Science Letters 224.

Wan, S.M., Kurschner, W.M., Clift, P.D., Li, A.C., Li, T.G., 2009. Extreme weathering/erosion during the Miocene Climatic Optimum: Evidence from sediment record in the South China Sea. Geophysical Research Letters 36.

Wang, E., Kamp, P.J.J., Xu, G., Hodges, K.V., Meng, K., Chen, L., Wang, G., Luo, H., 2015. Flexural bending of southern Tibet in a retro foreland setting. Scientific Reports 5.

Wang, Y., Zhang, L., Zhang, J., Wei, C., 2017. The youngest eclogite in central Himalaya: P–T path, U–Pb zircon age and its tectonic implication. Gondwana Research, v. 41, p. 188-206.

Warren, C.J., Grujic, D., Cottle, J.M., Rogers, N.W., 2012. Constraining cooling histories: rutile and titanite chronology and diffusion modelling in NW Bhutan. Journal of Metamorphic Geology 30.

Warren, C.J., Singh, A.K., Roberts, N.M.W., Regis, D., Halton, A.M., Singh, R.B., 2014. Timing and conditions of peak metamorphism and cooling across the Zimithang Thrust, Arunachal Pradesh, India. Lithos 200, 94-110.

Webb, A.A.G., 2013. Preliminary balanced palinspastic reconstruction of Cenozoic deformation across the Himachal Himalaya (northwestern India). Geosphere 9.

Webb, A.A.G., An, Y., Harrison, T.M., Julien, C., Burgess, W.P., 2007. The leading edge of the Greater Himalayan Crystalline complex revealed in the NW Indian Himalaya: Implications for the evolution of the Himalayan orogen. Geology 35, 955-958.

Webb, A.A.G., Yin, A., Dubey, C.S., 2013. U-Pb zircon geochronology of major lithologic units in the eastern Himalaya: Implications for the origin and assembly of Himalayan rocks. Geological Society of America Bulletin 125, 499-522.

Webb, A.A.G., Yin, A., Harrison, T.M., Célérier, J., Gehrels, G.E., Manning, C.E., Grove, M., 2011. Cenozoic tectonic history of the Himachal Himalaya (northwestern India) and its constraints on the formation mechanism of the Himalayan orogen. Geosphere 7.

Wortel, M.J., Spakman, W., 2000. Subduction and Slab Detachment in the Mediterranean-Carpathian Region. Science 290, 1910-1917.

Yan, D.-P., Zhou, M.-F., Robinson, P., Grujic, D., Malpas, J., Kennedy, A., Reynolds, P., 2012. Constraining the mid-crustal channel flow beneath the Tibetan Plateau: data from the Nielaxiongbo gneiss dome, SE Tibet. International Geology Review 54.

Yin, A., 1989. Origin of regional, rooted low-angle normal faults: a mechanical model and its tectonic implications. Tectonics 8, 469-482.

Yin, A., 2006. Cenozoic tectonic evolution of the Himalayan orogen as constrained by along-strike variation of structural geometry, exhumation history, and foreland sedimentation. Earth-Science Reviews 76.

Yin, A., Harrison, T.M., Murphy, M.A., Grove, M., Nie, S., Ryerson, F.J., Wang, X.F., Chen, Z.L., 1999. Tertiary deformation history of southeastern and southwestern Tibet during the Indo-Asian collision. Geological Society of America Bulletin 111.

Yin, A., Harrison, T.M., Ryerson, F.J., Chen, W., Kidd, W.S.F., Copeland, P., 1994. Tertiary structural evolution of the Gangdese thrust system, southeastern Tibet. Journal of Geophysical Research 99.

Yu, H., Webb, A.A.G., He, D., 2015. Extrusion vs. duplexing models of Himalayan mountain building 1: Discovery of the Pabbar thrust confirms duplex-dominated growth of the northwestern Indian Himalaya since Mid-Miocene. Tectonics 34, 313-333.

Zhang, L.-Y., Ducea, M.N., Ding, L., Pullen, A., Kapp, P., Hoffman, D., 2014. Southern Tibetan Oligocene–Miocene adakites: A record of Indian slab tearing. Lithos 210, 209-223.

Zhang, R., Murphy, M.A., Lapen, T.J., Sanchez, V., Heizler, M., 2011. Late Eocene crustal thickening followed by Early-Late Oligocene extension along the India-Asia suture zone: Evidence for cyclicity in the Himalayan orogen. Geosphere 7, 1249-1268.

## Figure Captions

**Fig. 1**. Schematic illustrations of models for the tectonic evolution of the Himalaya and the emplacement of its crystalline core. **A**. Emile Argand's (1924) model of India underthrusting Asia. **B**. Plate tectonic models (in this case, simplified from Dewey and Bird, 1970) largely match Argand's geometry, while considering dynamic elements such as slab detachment. A large variety of lithospheric-scale plate tectonic models have been proposed for the Himalayan-Tibetan system (e.g., the distributed vs. discrete deformation debates of England and Houseman (1986) vs. Peltzer and Tapponnier (1988), but these are roughly equivalent when focusing on the evolution of the Himalayan orogenic wedge. The models of Chemenda et al. (1995; 2000) are an exception, as explained in part D of this figure. **C**. Wedge extrusion models include the South Tibet fault as a north-dipping normal fault accommodating the southwards extrusion of the high-grade crystalline core of the Himalaya (i.e., the Greater Himalayan Crystalline complex / duplex, here labeled "GHC") from below a fold-thrust belt of Tethyan strata (i.e., the Tethyan Himalaya "TH") (e.g., Burchfiel and Royden, 1985). The Indus-Tsangpo suture ("ITS") marks the boundary between originally Asian and originally Indian rocks. **D**. Lithospheric-scale wedge extrusion models at lithospheric scale resulted from physical experiments by Chemenda et al. (1995; 2000), in which partially-subducted continental crustal slices detached from the down-going plate, in some cases in association with slab detachment, and buoyantly rose back to upper crustal levels between bounding thrust and normal faults. The physical models had many permutations, with some involving slab detachment, and the steep normal fault offers a potential South Tibet fault analogue. **E**. Channel flow – focused denudation models involve two main stages: first, southwards tunneling of a channel of partially molten lower / middle crustal rocks, and second, intensified monsoonal rains and resultant erosion forcing extrusion of these deep rocks and

continued rock supply via the channel to the extruding system (Nelson et al., 1996; Beaumont et al., 2001). **F**. Tectonic wedging models involve emplacement of the high-grade crystalline core of the Himalaya at depth, bound by a thrust and a backthrust (Yin, 2006; Webb et al., 2007). **G**. Duplexing models are similar to tectonic wedging models except that much of the crystalline core was developed by accretion of thrust slices from the downgoing Indian plate during the operation of the bounding thrust and backthrust systems (He et al., 2015).

**Fig. 2**. Simplified tectonic map of the Himalaya, and the same map with a data overlay. Age constraints on south Tibetan magmatism and activity along the South Tibet fault are plotted in map view here and in age vs. longitude space in Figure 3, and listed in Supplementary Tables 1 and 6. The gray and dark blue arcs show different radii of curvature for different segments of the mountain belt (Arc 1: R ≈ 2000 km; Arc 2: R ≈ 1200 km). The north-south breadth of the Kailas formation exposure is exaggerated for visibility (and included for its potential role in recording slab anchoring, see note 9 of Figure 6B). Geology along the India-Asia suture is after Aitchison et al. (2002; 2007), An et al. (2014), Ding et al. (2005); Henderson et al. (2011), and Pan et al. (2004). Geology of the Bhutan Himalaya is after Greenwood et al. (2016), Grujic et al. (2011), Kellett and Grujic (2012), and Regis et al. (2014). Geology of the western Himalaya is after Thakur and Rawat (1992), Webb et al. (2011) and Yu et al. (2015). The far northeastern exposures of the South Tibet fault are after Yan et al. (2012). The out-of-sequence thrust in eastern Nepal is after Ambrose et al. (2015) and Larson et al. (2016). Geology of all remaining regions is after previous compilations by He et al. (2015) and Webb (2013).

**Fig. 3**. Longitudinal variations in compiled age constraints on key Himalayan processes. **A**. South Tibetan magmatism shows increasingly younger ages from the ends of the range

towards the east-central Himalaya (see similar compilation by Leary et al., 2016). The plotted data are listed with sources in Supplementary Table 6. **B**. A metamorphic transition within the Greater Himalayan Crystalline duplex occurred ca. 27–26 Ma along the whole range, whereas the South Tibet fault ceased motion earliest in the far eastern and western Himalaya (at ca. 24–20 million years ago), and latest in the central eastern Himalaya (at 13–11 million years ago). Before the metamorphic transition, rocks in the Greater Himalayan Crystalline duplex record exclusively prograde metamorphism, whereas after the transition some rocks in this unit record prograde metamorphism and other rocks record retrograde metamorphism. Structurally higher rocks record the earliest retrograde metamorphism, and prograde-to-retrograde pressure-temperature paths generally get younger with increasing structural depth within the unit (e.g., Corrie and Kohn, 2011; Rubatto et al., 2013). Age data and sources for the metamorphic transition are listed in Supplementary Table 2; age data and sources for timing of cessation of South Tibet fault activity are listed in Supplementary Table 1. **C**. and **D**. Temporally constrained pressure and temperature estimates along decompression and cooling paths (respectively) across the structurally high (and northerly) portions of the Greater Himalayan Crystalline duplex are plotted. The longitude of each constraint is indicated via color, as keyed to a color spectrum. Data and sources are listed in Supplementary Table 3.

**Fig. 4**. Compilation of detrital thermochronology results from the Himalayan foreland basin. Detrital thermochronology involves sampling sedimentary materials and acquiring cooling ages from detrital components, in order to constrain the cooling history of the sediment source regions. In parts **A** and **B**, $^{40}Ar/^{39}Ar$ muscovite and fission track zircon results are plotted, respectively, for dates younger than 50 million years old. Given moderate to rapid cooling, closure of these systems occurs at ~425 °C and ~240 °C, respectively (Bernet and

Garver, 2005; Harrison et al., 2009). The data are shown using the Kernel Density Estimation (KDE) methodology, which plots the detrital dates as a set of Gaussian distributions (Vermeesch, 2004). This approach allows the age ranges and abundances of different detrital age populations to be compared: peaks in the curves represent peaks in the detrital age populations. For these plots, the population for a single sample is shown as a curve, sample longitude is keyed to a color spectrum, and the depositional age is shown via the squares at the young (left) terminations of the curve. A color spectra denotes longitude, with muscovite ages spanning from the western through central Himalaya and zircon ages extending somewhat farther to the east-central Himalaya. Data for each sample are plotted in isolation in Supplementary Figure 1, and data sources are listed in Supplementary Table 4. Part **B.ii.** shows the zircon fission track data for samples deposited from 15 Ma to 10 Ma, and highlights the highest probability peak for each sample. Similar plots for both data types and each available five million year interval are presented and discussed in Supplementary Figure 1.

**Fig. 5**. Schematic 3D diagram showing lateral propagation of slab detachment from both west and east across the Himalayan system. Shaded red colors represent the upper surface of the descending Indian plate. Slab detachment affects topographic evolution by releasing the vertical traction excited by the subducting slab, thereby releasing the dynamic deflection, and increasing the vertical load in adjacent regions where the slab remains attached (depending on the slab to mantle viscosity ratio), thereby possibly producing dynamic subsidence. This results in a wave of uplift from the edges towards the center of the chain, possibly following an early episode of subsidence. The lateral propagation of slab detachment also bends orogenic belts, as shown here and explained in the text. The tighter curvature of the eastern Himalaya (see also Figure 2) reflects the slower propagation of slab detachment here.

**Fig. 6**. **A**. Proposed Himalayan tectonic and topographic evolution from 30 to 10 million years ago (Ma), shown in schematic true-scale cross-sections across five million year increments accompanied by topographic profiles with 10x vertical exaggeration. Differences in western and east-central Himalayan evolution are documented via representative sections at ~77°E and ~90°E (present coordinates) at 20 Ma, 15 Ma, and 10 Ma. Mantle flow is schematically represented as grey arrows. The dynamic deflection shows the model results from Husson et al. (2014) as blue curves. The 30 Ma time period represents a geometry not considered by Husson et al. (2014), so the dynamic deflection for this period is estimated and represented by a dashed blue curve. The modeled time period spans anchoring of the subducted Indian lithosphere, lateral migration of slab detachment, and the progressive re-initiation of Indian lithosphere underthrusting. **B**. An annotated description of the tectonic model presented in part A.

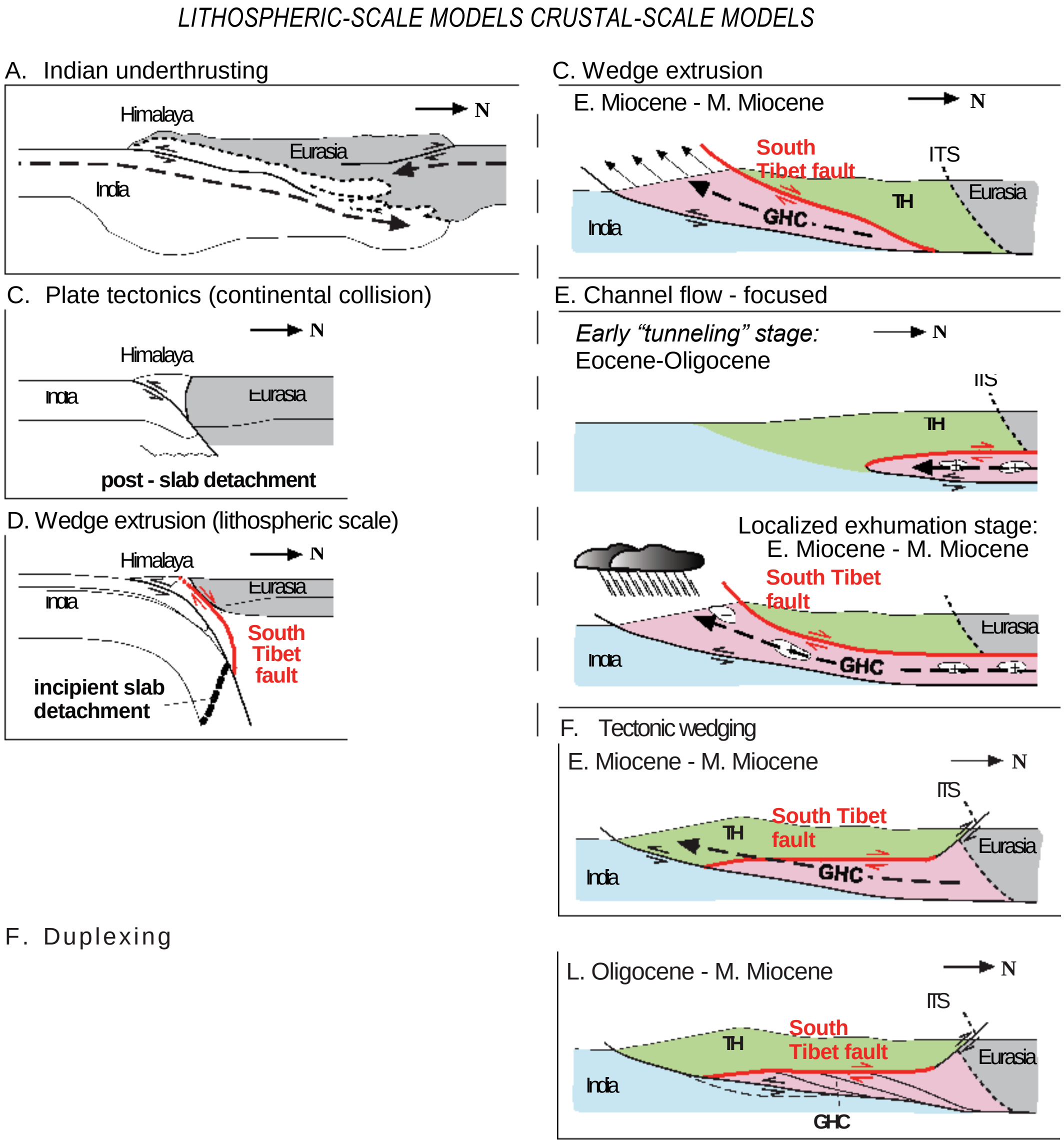


Figure 1, Webb et al.

Click here to download Figure Figure 2 - HimMap 170302.pdf

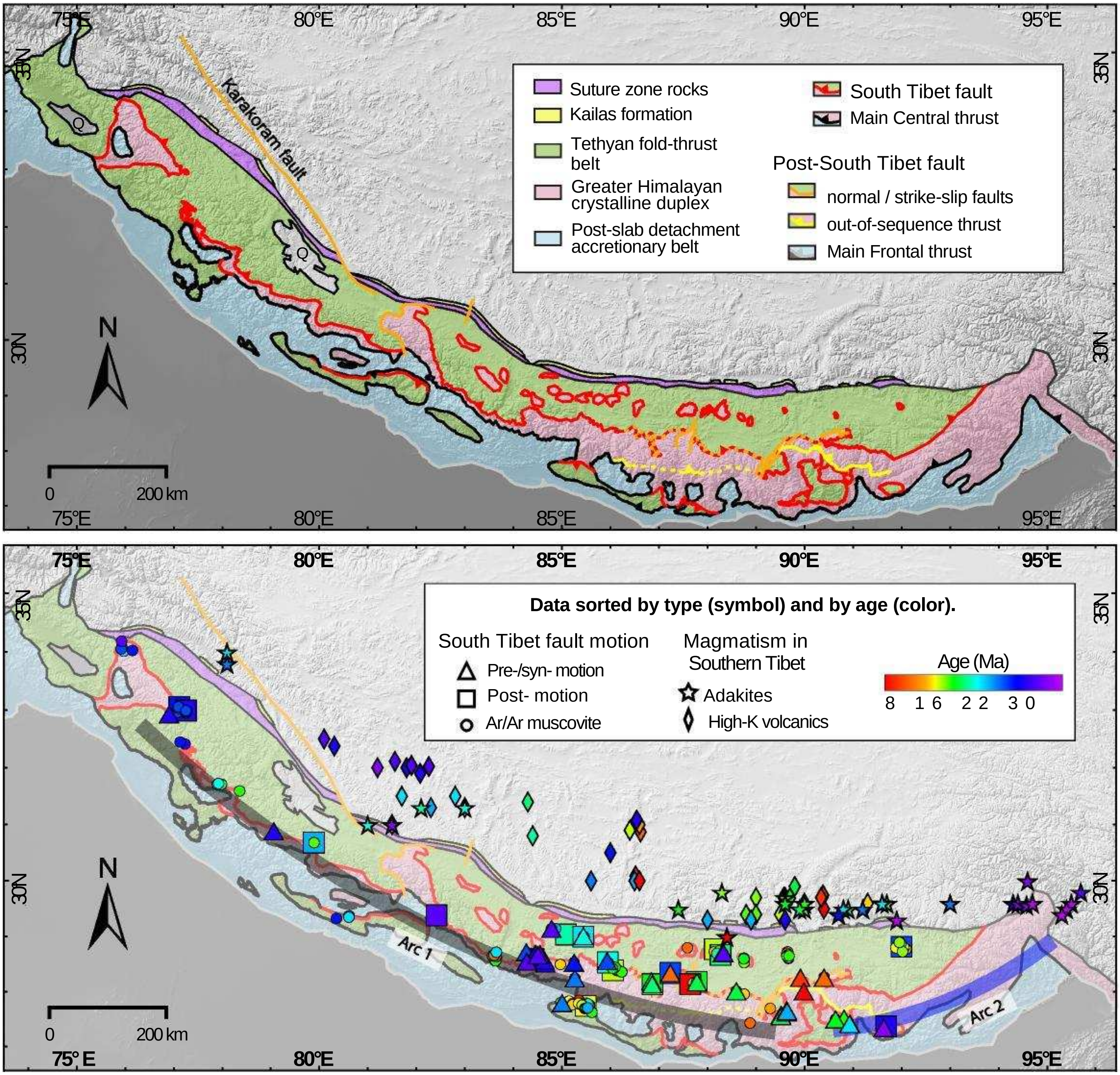


Figure 2, Webb et al.

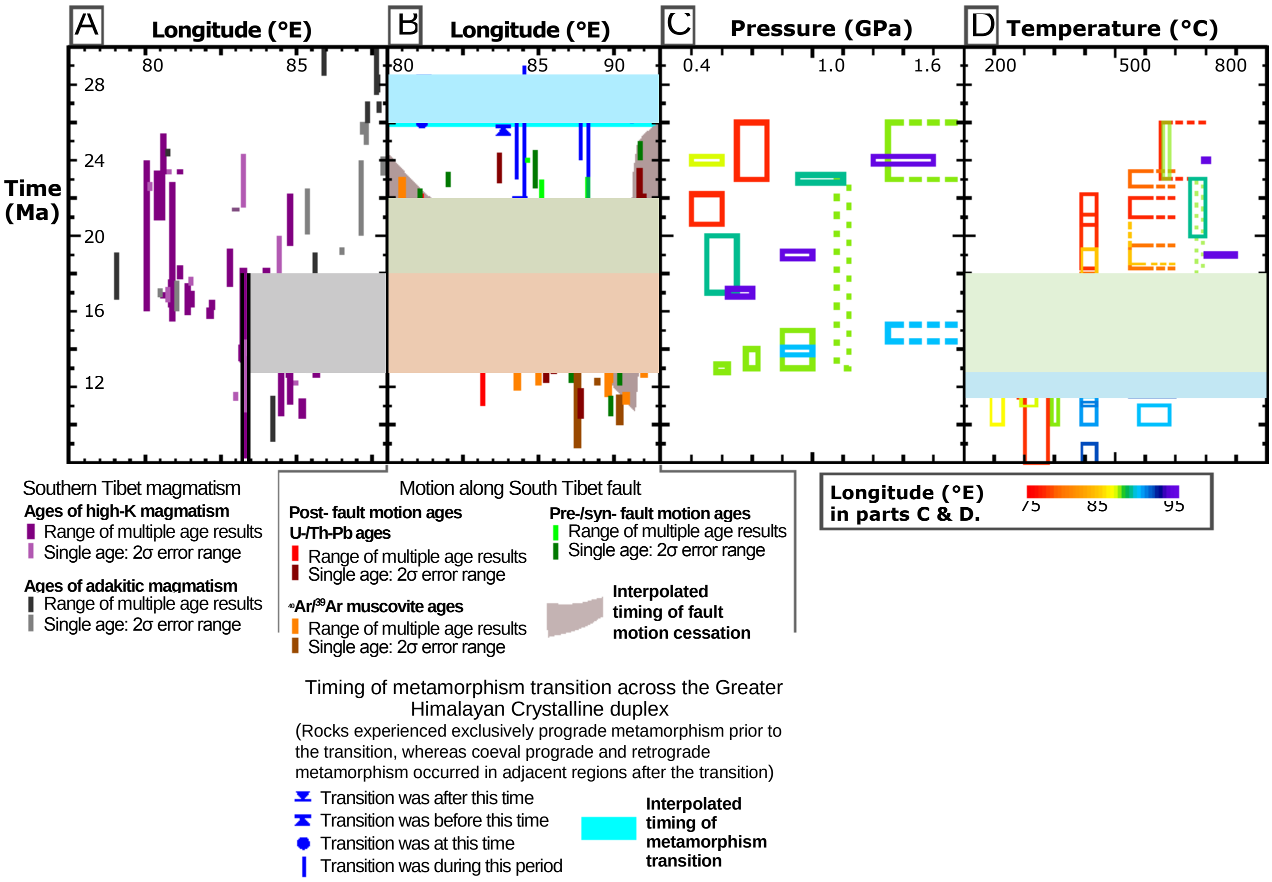


Figure 3, Webb et al.

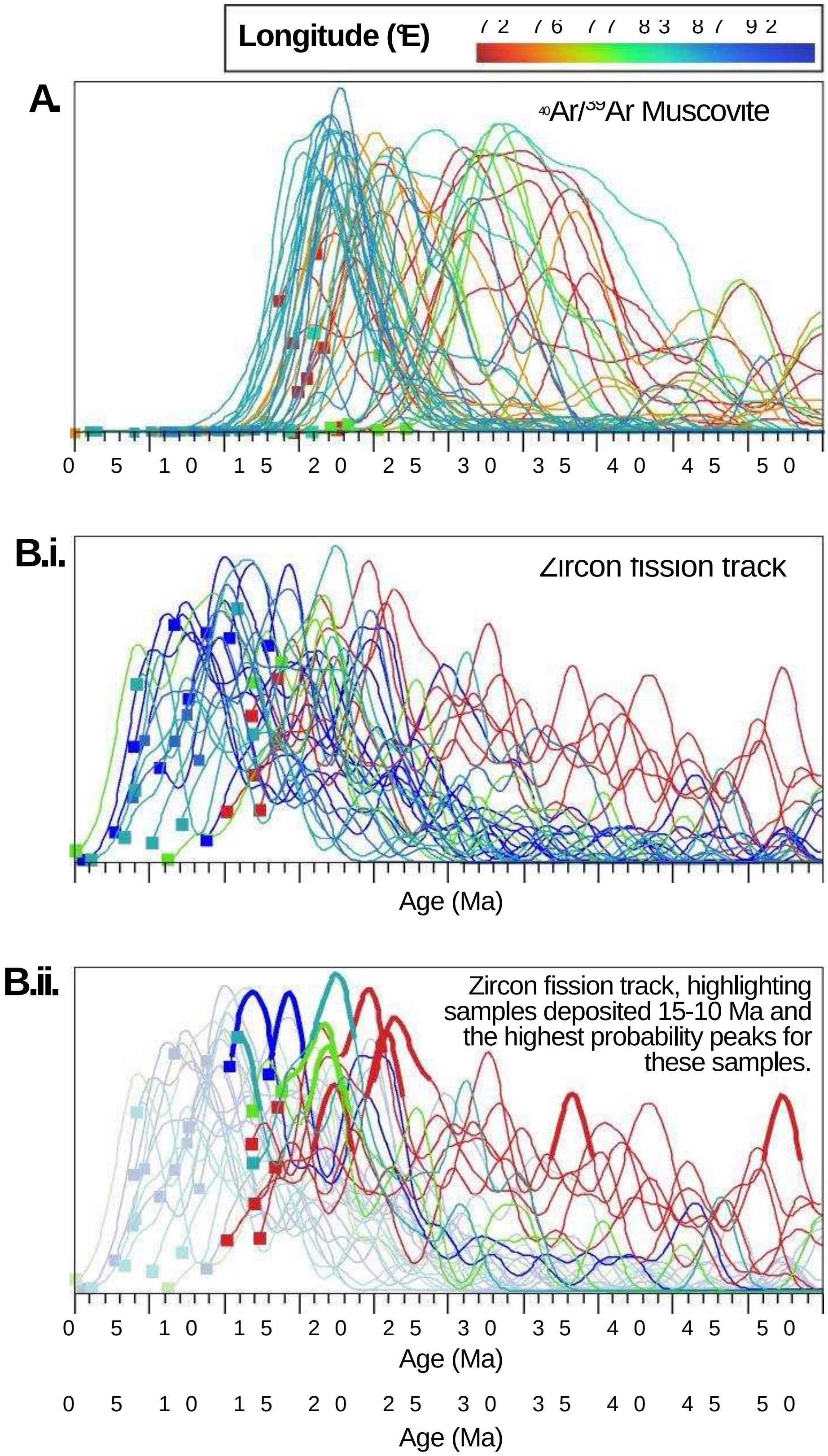


Figure 4, Webb et al.

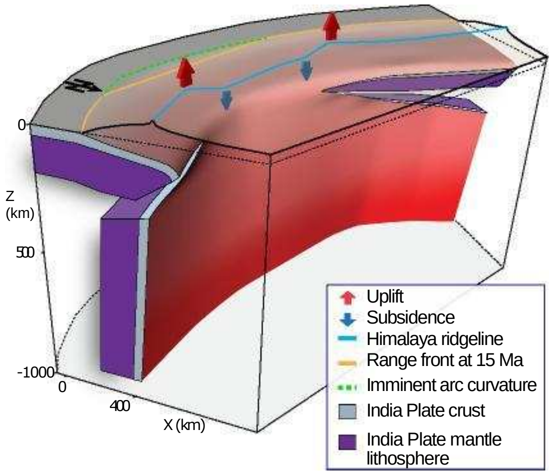


Figure 5, Webb et al.

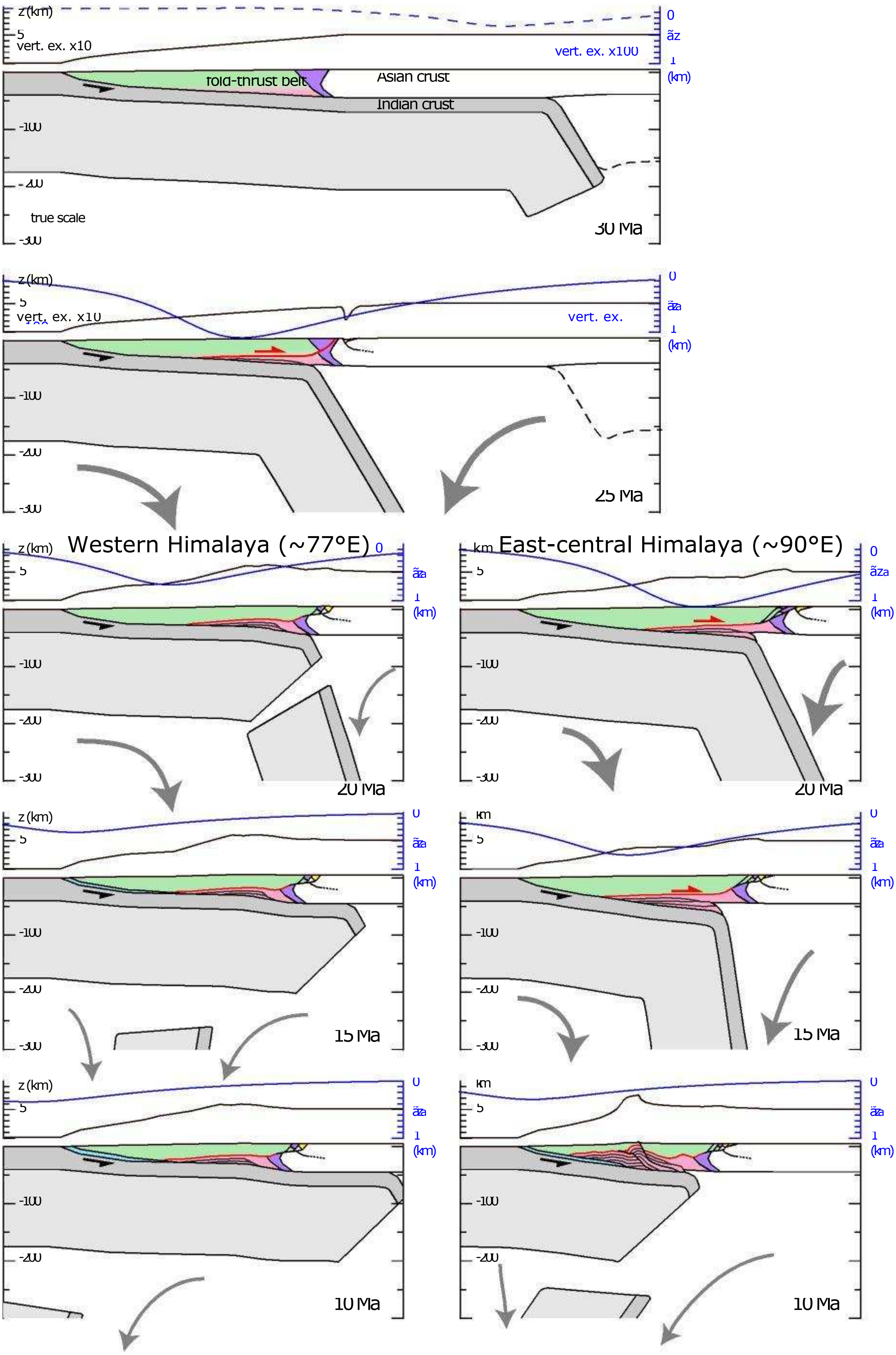


Figure 6A, Webb et al.

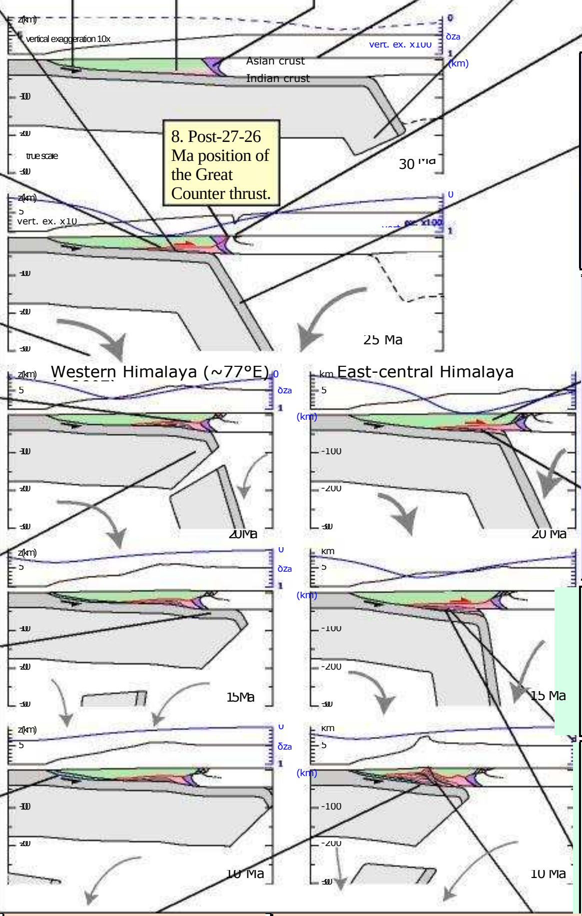


1. The Indian crust thinned beneath the front of the Himalaya as the upper portions of it were scraped off and incorporated into the fold-thrust belt.

2. The Himalayan orogenic wedge was not yet partitioned by the South Tibet fault at 30 Ma. The lowermost Tethyan fold-thrust belt and uppermost Greater Himalayan Crystalline duplex experienced similar peak conditions of ~1.0-0.8 GPa and ~650-600 °C (e.g., Vannay and Grasemann, 1998), so we estimate a transitional depth of ~30 km.

3. The suture zone rocks include ophiolite, melange, and pre-collisional forearc strata.

4. Thermo-chronologic records show that the Asian crust of the southern and central Tibetan Plateau was high and thus likely thick by ~45 Ma (Rohrmann et al., 2012).

5. The northern limits of underthrust and subducted Indian lithosphere are estimated from (a) surface volcanic records (DeCelles et al., 2011) and (b) the size of the detached Indian slab as imaged via seismic tomography (Replumaz et al., 2010).

6. The Greater Himalayan Crystalline duplex began to accrete material from the downgoing Indian plate along deep portions of the orogenic wedge at ~27-26 Ma, as interpreted from metamorphic patterns. The Himalayan metamorphic rocks record only prograde metamorphism until ~27-26 Ma, at which point initial decompression and retrogressive metamorphism occurred in the structurally highest Greater Himalayan Crystalline duplex rocks along the length of the orogen (see Figure 3B, Supplementary Table 2). This decompression is interpreted to record uplift and exhumation in response to deep duplexing; the duplexing initiated in response to steepening of the sole thrust in response to slab anchoring. Steepening of the sole thrust would encourage vertical thickening processes like duplexing in order to maintain a stable orogenic wedge (Davis et al., 1983; Dahlen, 1984).

7. Backthrusting along the South Tibet fault became active as slab anchoring steepened the sole thrust at ~27-26 Ma, whereupon the thrust wedge shortened and thickened (see note 6 directly above). Top-to-the-north backthrusting extended northwards from the Himalayan sole thrust and linked with the top-to-the-north Great Counter thrust system along the suture zone (Yin et al., 1994; 1999; Webb et al., 2007; He et al., 2016).

8. Post-27-26 Ma position of the Great Counter thrust.

9. Early Kailas conglomerate deposition occurred at ~26 Ma in [A] a normal fault basin caused by changes in South Tibetan crustal boundary conditions during rollback, as shown here (DeCelles et al., 2011; Carrapa et al., 2014), or [B] a thrust foreland basin (Yin et al., 1994; 1999; Wang et al., 2015).

10. Southwards migration of volcanism from ~30 Ma to ~25 Ma tracks anchoring of the Indian lithospheric slab (DeCelles et al., 2011). Although this relative rollback faltered along the India-Asia margin at ~25 Ma, it likely persisted across the oceanic lithosphere to the east and west of the Indian continent (e.g., Replumaz et al., 2014; Capitanio et al., 2015). This tore the slab vertically at the ends of the Himalaya, and may have initiated sub-horizontal slab tears that accommodated the lateral propagation of slab detachment.

11. After the main anchoring phase and prior to slab detachment, the South Tibet fault (and its northern surface expression, the Great Counter thrust system) was active and material accreted to the deep portions of the Himalayan orogenic wedge along the sole thrust. In the western Himalaya, the period between anchoring and slab breakoff was relatively brief as the lateral propagation of slab detachment from west to east proceeded rapidly.

12. At ~77°E, slab breakoff occurred just prior to ~20 Ma. With the release of the release of the dynamic traction of the slab and the relative southwards translation of the slab weight, the range and its underlying lithosphere uplifted towards isostatic equilibrium. Topography across the range increased, and the shallowing of the sole thrust caused cessation of deep accretion and South Tibet fault (and Great Counter thrust) motion.

13. Underthrusting of Indian lithosphere below Asian crust resumed after slab breakoff.

14. The period after the main anchoring phase and before slab breakoff was much longer in the east-central Himalaya (~90°E) than in the western Himalaya. In the east-central Himalaya, this period is 14-12 million years, whereas in the west this period is <~6 million years. As in the west, during this period the South Tibet fault (and its northern surface expression, the Great Counter thrust) was active and material accreted to the deep portions of the Himalayan orogenic wedge along the sole thrust.

15. Duplexing occurred as the sole thrust steepened in response to increasing slab pull. South Tibet fault motion accommodated duplex growth as a roof backthrust. Thrust sheets accreted at depth became progressively lower levels of the Greater Himalayan Crystalline duplex. The younging with structural depth (now preserved as younging-to-the-south in dominantly northwards-tilted Greater Himalayan Crystalline duplex sections) is recorded by prograde-to-retrograde metamorphic cycles, which young to the south across thrust sheets (e.g., Carosi et al., 2010; Corrie and Kohn, 2011; Imayama et al., 2012; Montomoli et al., 2013; Ambrose et al., 2015; Larson et al., 2015).

16. Underthrusting of Indian lithosphere below Asian crust continued here at 15 Ma, even as the slab had not yet broken off in the east-central Himalaya.

17. Because deep duplexing persisted for a relatively long period in the east-central Himalaya, it built a much thicker Greater Himalayan Crystalline duplex versus the western Himalaya. The strong slab pull experienced by the east-central Himalaya immediately prior to final slab detachment produced a deep, steeply dipping Himalayan sole thrust.

18. The increasing steepness of the Himalayan sole thrust in the east-central Himalaya prior to final slab breakoff brought large portions of the Greater Himalayan Crystalline complex here to depths of eclogite facies metamorphism. This can explain why Miocene ecologite facies metamorphism along the arc appears limited to the east-central Himalaya (Grujic et al., 2011; Wang et al., 2017).

19. Underthrusting of Indian lithosphere below Asian crust continued here at 10 Ma, and is maintained to the present. After final detachment of the Indian slab in the east-central Himalaya at 13-11 Ma, the range achieved an overall maximum of topography for the whole arc. The topographic maximum likewise intensified the South Asian monsoon to a maximum (Boos and Kuang, 2010), thereby encouraging increased precipitation and orographically-controlled erosion. We speculate that this intensified erosion produced increasingly vertically-stacked duplexing of thrust sheets accreted to the orogenic wedge after slab detachment (a la Konstantinovskaia and Malavieille, 2005), which may have resulted in a positive feedback loop maintaining Himalayan topography. In this hypothesis, erosion-forced thrust duplexing increased topography, and increased topography maintained a relatively strong South Asian monsoon along with associated orographic precipitation and resultant high erosion.

20. At ~90°E, slab breakoff occurred at 13-11 Ma. As in the other portions of the range, with the release of the the dynamic traction of the slab and the relative southwards translation of the slab weight, the range and its underlying lithosphere uplifted towards isostatic equilibrium. Here too, topography increased, and the shallowing of the sole thrust caused cessation of [A] deep accretion (duplexing) and [B] South Tibet fault (and Great Counter thrust) motion.

21. An out-of-sequence thrust (e.g., Grujic et al., 2011) and a steeply dipping normal fault (e.g., Kellett and Grujic, 2012; Kellett et al., 2013) observed in the east-central Himalaya may record a structural response to final slab breakoff here at 13-11 Ma. Both faults were likely active at this time (Kellett and Grujic, 2012). Such extruding wedge dynamics have been physically modeled and considered in contexts of other Himalayan tectonic events (e.g., Chemenda et al., 1995; 2000; see Figure 1D). This extrusion would enhance and localize topographic uplift in response to slab detachment.

Figure 6B, Webb et al.